Base editing correction of hypertrophic cardiomyopathy in human cardiomyocytes and humanized mice

Base Editing Correction of Hypertrophic Cardiomyopathy in Human Cardiomyocytes and Humanized Mice

Andreas C. Chai[1,2], Miao Cui[1,2], Francesco Chemello[1,2], Hui Li[1,2], Kenian Chen[3], Wei Tan[1,2], Ayhan Atmanli[1,2], John McAnally[1,2], Yu Zhang[1,2], Lin Xu[3], Ning Liu[1,2], Rhonda Bassel-Duby[1,2], and Eric N. Olson[1,2*]

[1]Department of Molecular Biology, University of Texas Southwestern Medical Center, Dallas, TX USA.

[2]Hamon Center for Regenerative Science and Medicine, University of Texas Southwestern Medical Center, Dallas, TX USA.

[3]Quantitative Biomedical Research Center, Department of Population and Data Sciences, University of Texas Southwestern Medical Center, Dallas, TX USA.

*Corresponding author. Email: Eric.Olson@utsouthwestern.edu

Abstract

The most common form of genetic heart disease is hypertrophic cardiomyopathy (HCM), which is caused by variants in cardiac sarcomeric genes and leads to abnormal heart muscle thickening. Complications of HCM include heart failure, arrhythmia, and sudden cardiac death. The dominant-negative c.1208 G>A (p.R403Q) pathogenic variant (PV) in β-myosin (*MYH7*) is a common and well-studied PV that leads to increased cardiac contractility and HCM onset. Here we identify an adenine base editor (ABE) and single-guide RNA system that can efficiently correct this human PV with minimal bystander editing and off-target editing at selected sites. We show that delivery of base editing components rescues pathological manifestations of HCM in induced pluripotent stem cell (iPSC)-cardiomyocytes derived from HCM patients and in a humanized mouse model of HCM. Our findings demonstrate the use of base editing to treat inherited cardiac diseases and prompt the further development of ABE-based therapies to correct a variety of monogenic variants causing cardiac disease.

Main

Hypertrophic cardiomyopathy (HCM), a disease of abnormal heart muscle thickening, is the most common form of genetic heart disease in the United States, affecting upwards of 1 in 200 people [1,2]. Clinical complications of HCM include heart failure, arrhythmia, and sudden cardiac death. There is no cure for HCM, aside from heart transplant, which presents its own complications and requires lifetime immunosuppression. While HCM-causing variants are found in various sarcomeric protein-encoding genes, over one-third of all HCM-causing variants occur in the Myosin Heavy Chain 7 (*MYH7*) gene, which encodes ~~for~~ β-myosin heavy chain, a motor ATPase that incorporates into the thick filament of cardiac muscle and plays a major role in cardiac contraction. These pathogenic variants are generally autosomal dominant missense variants, which allow the incorporation of pathogenic myosin heads into cardiac sarcomeres and lead to increased energy consumption, hypercontractility, and disease progression of HCM [3].

The heterozygous *MYH7* c.1208 G>A (p.R403Q) pathogenic missense variant causes severe HCM with early-onset and progressive myocardial dysfunction and has a high incidence of early sudden cardiac death as fifty percent of patients die by 40 years of age [4,5]. It was the first *MYH7* variant linked to HCM, leading to the discovery of multiple other missense variants in cardiac sarcomere genes and generating numerous studies of its function. The R403Q missense variant, located on the myosin mesa of the myosin head, results in a loss of positive charge on the myosin head, weakening its interaction with myosin binding protein-C, a molecular brake, and leading to an increase in the number of functionally accessible myosin heads available for contraction that pathologically augments sarcomere contractility [6]. This poison peptide effect results in a dominant-negative disease that requires direct correction or ablation of the pathogenic allele.

51 Base editing has emerged as an attractive method to correct and potentially cure genetically
52 based diseases, especially single nucleotide variants. Base editors are fusion proteins of Cas9
53 nickase or deactivated Cas9 and a deaminase protein, which allow base pair edits without double-
54 strand breaks within a defined editing window in relation to the protospacer adjacent motif (PAM)
55 site of a single-guide RNA (sgRNA) [7,8]. Adenine base editors (ABEs) use deoxyadenosine
56 deaminase to convert DNA A•T base pairs to G•C base pairs via an inosine intermediate and have
57 been previously shown to function in many post-mitotic cells in vivo and in vitro [9-11].

58 Here, we and colleagues who authored the accompanying manuscript (Reichart, Newby,
59 Wakimoto, et al.)[12] report the use of different gene editing strategies to correct the *MYH7* c.1208
60 G>A (p.R403Q) pathogenic missense variant. We develop an ABE-mediated strategy that
61 efficiently corrects and rescues pathological phenotypes of HCM in patient-derived cells.
62 Furthermore, we generate a humanized mouse model containing the pathogenic missense variant
63 with sequence complementarity to the human sgRNA and show that postnatal ABE correction of
64 this mouse model prevents HCM onset.

65

66 **Results**

67 **Identification of an ABE to correct the R403Q pathogenic variant in human iPSCs**

68 To screen various ABEs for their efficiencies, we first inserted the *MYH7* c.1208 G>A (p.R403Q)
69 pathogenic missense variant using CRISPR-Cas9-based homology-directed repair in a human
70 induced pluripotent stem cell (iPSC) line derived from a healthy donor (HD^{WT}). We isolated an
71 isogenic heterozygous clone ($HD^{403/+}$) that mirrors the heterozygous genotype found in patients [4],
72 as well as an isogenic homozygous clone ($HD^{403/403}$) that has not been previously described in
73 patients. Sequencing confirmed no mutations on the highly homologous *MYH6* gene during

74 generation of these clones, and these iPSCs readily differentiate into cardiomyocytes (CMs)
75 (**Extended Data Fig. 1**).

76 As ABEs have an optimal activity window in protospacer positions 14-17 (counting the
77 first nucleotide immediately 5' of the PAM sequence as protospacer position 1), we chose a sgRNA
78 with an NGA PAM that places the *MYH7* c.1208 G>A pathogenic variant in protospacer position
79 16 (h403_sgRNA) (**Fig. 1a**). To identify an optimal ABE capable of efficiently correcting the
80 pathogenic nucleotide back to the wildtype nucleotide without introducing any bystander edits, we
81 tested various engineered deaminases including either ABEmax [13], which is an optimized, narrow-
82 windowed ABE7.10 variant, or ABE8e [14], which is a highly processive, wide-windowed, evolved
83 ABE7.10 variant. Each engineered deaminase variant was fused to engineered SpCas9 variants
84 including SpRY, which targets NRN PAMs [15]; SpG, which targets NGN PAMs [15]; SpCas9-NG,
85 which targets NG PAMs [16]; or SpCas9-VRQR, which targets NGA PAMs [17]. We then screened
86 these ABEs for their efficiency of correction in our HD$^{403/403}$ iPSC line via transient transfection
87 with h403_sgRNA (**Fig. 1b**). We selected the HD$^{403/403}$ iPSC line for screening to ensure that all
88 G nucleotide Sanger sequencing reads at position c.1208 are due to ABE editing. Similar editing
89 efficiency of the pathogenic adenine was achieved with all ABEmax-SpCas9 variants tested,
90 ranging from 26 ± 2.3% with ABEmax-SpRY to 34 ± 2.5% with ABEmax-VRQR, with minimal
91 bystander editing of neighboring adenines (the average across three bystanders was 2.6 ± 1.7%).
92 ABE8e-SpCas9 variants achieved higher editing efficiencies, ranging from 27 ± 2.6% with
93 ABE8e-SpRY to 37 ± 1.5% with ABE8e-SpG, with slightly increased bystander editing of
94 neighboring adenines (the average across three bystanders was 4.0 ± 2.0%) (**Fig. 1c**). These
95 bystander edits are predicted to result in K405E, K405R, or K405G variants in β-myosin heavy
96 chain depending on the combination of edits, which may be deleterious due to the high intolerance

97 of *MYH7* for missense variants [18], although the consequences of these variants on β-myosin heavy
98 chain function have not been described. For subsequent experiments, we opted to use the more
99 narrow-windowed ABEmax to reduce potential bystander edits, and the SpCas9-VRQR variant
100 with its more stringent PAM requirements to reduce potential Cas-dependent off-target editing.
101

102 **Correction efficiency and off-target DNA editing analysis in HCM patient-derived iPSCs.**
103 To apply our ABEmax-VRQR and h403_sgRNA system to a disease model, we derived human
104 induced pluripotent stem cells (iPSCs) from two HCM patients with the *MYH7*$^{403/+}$ pathogenic
105 variant (HCM1$^{403/+}$ and HCM2$^{403/+}$) and corrected the *MYH7*$^{403/+}$ variant via plasmid nucleofection
106 of ABEmax-VRQR-P2a-EGFP and h403_sgRNA, and fluorescence-activated cell sorting of GFP^{+}
107 cells (**Fig. 2a**). By high throughput sequencing (HTS), despite 98-99% on-target editing, we
108 observed minimal to no off-target DNA editing (0.12% or less) at all 58 adenine bases for eight
109 tested candidate off-target loci, which were identified using the bioinformatic tool CRISPOR [19]
110 (**Fig. 2b**, and **Extended Data Fig. 2**). A low frequency (0.03-0.48%) of bystander editing was
111 observed at the three bystander adenines for amino acid 505 (K505) of β-myosin. We isolated
112 corrected clonal lines of the HCM patient-derived iPSCs (HCM1^{WT} and HCM2^{WT}) containing no
113 bystander edits or editing of the highly homologous *MYH6* gene, ensuring that subsequent
114 characterizations are due to correction of the pathogenic nucleotide. These results suggest that
115 h403_sgRNA with ABEmax-VRQR can efficiently and specifically correct the target pathogenic
116 missense variant with minimal bystander editing and little to no DNA editing at tested off-target
117 sites.
118

119 **Functional analyses of ABE-corrected patient-derived iPSC-CMs**

120 In individual CMs, the *MYH7* p.R403Q pathogenic variant increases the number of functional
121 myosin heads available for contraction, which leads to increased force generation and greater ATP
122 consumption. Increases in both force generation and energy consumption have been previously
123 shown in isogenic iPSC-CMs engineered to have the R403Q pathogenic variant from a WT line
124 [20-22]. To determine if these previously validated changes are rescued in our corrected HCM patient-
125 derived iPSC-CMs, we differentiated both $MYH7^{403/+}$ pathogenic and $MYH7^{WT}$ healthy clonal lines
126 for all three patient-derived lines (HD, HCM1, and HCM2) into CMs (**Fig. 2a**).

127 To investigate whether gene editing correction could reduce hypercontractile force
128 generation in our HCM patient-derived lines, we plated iPSC-CMs at single-cell density on soft
129 polydimethylsiloxane surfaces, recorded high frame-rate videos of contracting CMs, and
130 calculated peak systolic force. The $HD^{403/+}$ iPSC-CMs showed a 1.7-fold increase in peak systolic
131 force compared to HD^{WT} iPSC-CMs originally derived from a healthy donor, consistent with
132 reports of a single *MYH7* p.R403Q variant being sufficient to lead to hypercontractility [6,22]. On the
133 other hand, corrected $HCM1^{WT}$ and $HCM2^{WT}$ CMs showed a 2.0-fold and 1.6-fold decrease in peak
134 systolic force, respectively, compared to their isogenic $HCM1^{403/+}$ and $HCM2^{403/+}$ counterparts.
135 (**Fig 2c**).

136 As previous studies have shown that the p.R403Q HCM variant leads to increased ATP
137 consumption and altered cellular metabolism [23], we next assessed changes in cellular energetics
138 via metabolic flux assays following gene editing correction. Basal oxygen consumption rates
139 (OCR) were increased 1.6-fold in $HD^{403/+}$ iPSC-CMs compared to HD^{WT} iPSC-CMs, and $HD^{403/+}$
140 iPSC-CMs had a 2.1-fold increase in maximum OCR compared to HD^{WT} iPSC-CMs. Corrected
141 $HCM1^{WT}$ and $HCM2^{WT}$ CMs showed a 1.4-fold and 1.2-fold reduction in basal OCR, respectively,
142 and a 3.7-fold and 2.1-fold reduction in maximum OCR, respectively, compared to isogenic

143 HCM1$^{403/+}$ and HCM2$^{403/+}$ CMs (**Fig. 2d**). These data demonstrate that correction of the
144 pathogenic variant in human HCM CMs is sufficient to rescue the hypercontractility phenotype
145 and restore normal cellular energetics.
146

147 **Development of a humanized mouse model of HCM**

148 We next sought to apply base editing to a mouse model of HCM. While β-myosin heavy chain is
149 the dominant myosin isoform found in adult human hearts, the highly homologous α-myosin heavy
150 chain is the dominant myosin isoform expressed in adult mouse hearts and is encoded by the *Myh6*
151 gene [24]. Consequently, previously described mouse models for HCM have placed the
152 corresponding human *MYH7* variant on the mouse *Myh6* gene to account for these expression
153 differences. While the 35 amino acids around R403 are 100% identical between human *MYH7* and
154 mouse *Myh6*, the DNA sequence encoding this region of the protein is not identical (**Extended**
155 **Data Fig. 3**). Thus, sgRNAs and editing strategies developed for the human genome would not be
156 directly applicable to a mouse model.

157 To perform preclinical studies using our human sequence-specific base editing strategy,
158 we generated a humanized mouse model containing the *MYH7* c.1208 G>A (p.R403Q) human
159 missense variant within the mouse *Myh6* gene that also has human DNA sequence identity of at
160 least 21 nucleotides upstream and downstream from the pathogenic variant to allow testing of
161 human genome specific CRISPR strategies (**Fig. 3a**). The other *Myh6* allele contained the
162 unmodified mouse genomic sequence. This humanized mouse model (*Myh6*$^{h403/+}$) mirrors the
163 phenotype of previously described *Myh6* p.R403Q mouse models [25,26]. Most notably, homozygous
164 mice (*Myh6*$^{h403/h403}$) have enlarged atria, extensive interstitial fibrosis, and die within the first week
165 of life (**Fig. 3b**). At 9 months of age, *Myh6*$^{h403/+}$ mice have developed cardiomyopathy with

166 significant ventricular hypertrophy, myocyte disarray, and fibrosis (**Fig. 3c**).

167

168 **In vivo ABE treatment of a mouse model of human HCM**

169 We packaged ABEmax-VRQR and h403_sgRNA within adeno-associated virus (AAV), a US
170 Food and Drug Administration approved viral delivery method. We chose to use the AAV9 capsid
171 due to its high cardiac transduction and use in clinical trials [27]. As the full-length base editor (~5.4
172 kb) exceeds the packaging limit of a single AAV9 (~4.7 kb), we split the base editor across two
173 AAV9s and used *trans*-splicing inteins to reconstitute the full-length base editor in cells upon
174 protein expression [28]. As AAV9 contains broad tissue tropism, we utilized a cardiac troponin T
175 (cTnT) promoter to limit expression of the base editor to CMs [29]. For this dual AAV9 system, each
176 AAV9 also contained a single copy of an expression cassette encoding h403_sgRNA (**Fig. 4a**).

177 We first sought to validate the efficiency of our dual AAV9 ABE system by trying to rescue
178 *Myh6*$^{h403/h403}$ mice, which die within the first week of life. Notably, no human patients have been
179 reported to have the homozygous genotype. We injected P0 (postnatal day 0) *Myh6*$^{h403/h403}$ pups
180 intrathoracically with either saline, a low dose (4×10^{13} vg/kg), or a high dose (1.5×10^{14} vg/kg) of
181 each AAV9 (total of 8×10^{13} vg/kg for low, and 3×10^{14} vg/kg for high) and monitored their
182 development (**Extended Data Fig. 4a**). The 3×10^{14} vg/kg high dose is the highest dose
183 administered in clinical trials [30]. The *Myh6*$^{h403/+}$ and *Myh6*^{WT} mice survived past weaning and well
184 into adulthood. The median survival of saline-injected *Myh6*$^{h403/h403}$ mice was 7.0 days, whereas
185 that of low-dose ABE-treated *Myh6*$^{h403/h403}$ mice was increased to 9.0 days (1.3-fold longer,
186 $P<0.05$ by Mantel-Cox test). The median survival of high-dose ABE-treated *Myh6*$^{h403/h403}$ mice
187 was increased to 15.0 days (2.1-fold longer, $P<0.01$ by Mantel-Cox test) (**Extended Data Fig.
188 4b**). Sanger sequencing of cDNA of the heart from a high-dose mouse indicated 35% correction

of the pathogenic nucleotide at the transcript level, suggesting that our dual AAV9 ABE system enabled editing in the heart (**Extended Data Fig. 4**).

As the *MYH7* p.R403Q variant only exists in a heterozygous form in human patients, we next deployed our dual AAV9 ABE system to prevent HCM disease onset in *Myh6*$^{h403/+}$ mice. We injected *Myh6*$^{h403/+}$ P0 pups intrathoracically with either saline or 1×10^{14} vg/kg of each AAV9 (2×10^{14} vg/kg total) and their littermate *Myh6*^{WT} control pups with saline. At 5 weeks of age, the mice were put on a chow diet containing 0.1% cyclosporine A, which has previously been shown to accelerate the onset of HCM in mouse models of sarcomere pathogenic variants [31]. Serial echocardiograms were conducted at 8, 12, and 16 weeks of age to monitor disease progression (**Fig. 4b**). We found that *Myh6*$^{h403/+}$ mice had increased features of HCM compared to *Myh6*^{WT} controls, including increased left ventricular anterior wall thickness at diastole (LVAW;d) (1.07 ± 0.0443 mm vs. 0.883 ± 0.0441 mm, P = 0.017) and increased left ventricular posterior wall thickness at diastole (LVPW;d) (1.04 ± 0.0809 mm vs. 0.867 ± 0.0590 mm, P = 0.128). These mice also had decreased left ventricular internal diameter at diastole (LVID;d) (2.34 ± 0.142 mm vs. 2.81 ± 0.0540 mm, P = 0.015) and systole (LVID;s) (0.940 ± 0.0713 mm vs. 1.24 ± 0.0520, P = 0.010), with ~~slightly~~ increased ejection fraction (EF) and fractional shortening (FS). The increased ventricular wall thickness and a concomitant decrease in ventricular diameter of *Myh6*$^{h403/+}$ mice, along with high-normal fractional shortening is consistent with the clinical progression in human patients [1].

In contrast, ABE-treated *Myh6*$^{h403/+}$ mice had reduced features of HCM with ~~comparable~~ similar echocardiographic measurements to *Myh6*^{WT} control mice, suggesting that gene correction of the pathogenic nucleotide was sufficient to prevent the onset of HCM (**Fig. 4c-h, Table 1,** and **Extended Data Fig. 5**). Histological analysis also revealed increased cardiac wall thickness and

212 decreased ventricular ~~diameter~~ cross-sectional area in *Myh6*$^{h403/+}$ mice compared to *Myh6*^{WT}
213 control mice, while ABE-treated *Myh6*$^{h403/+}$ mice had similar cardiac dimensions to *Myh6*^{WT}
214 control mice (**Fig. 4i-k**). When normalized to tibia length, *Myh6*$^{h403/+}$ mice had 1.3-fold larger
215 hearts by heart weight compared to *Myh6*^{WT} control mice, while ABE-treated *Myh6*$^{h403/+}$ mice had
216 no significant difference in heart weight compared to *Myh6*^{WT} mice (**Fig. 4l**). As a measure of
217 fibrosis, hearts from *Myh6*$^{h403/+}$ mice had 3.0-fold more collagen area compared to *Myh6*^{WT} control
218 mice, while ABE-treated *Myh6*$^{h403/+}$ mice had no significant difference in collagen area compared
219 to *Myh6*^{WT} mice (**Fig. 4m**). These data suggest that dual AAV9 ABE treatment was sufficient to
220 prevent the onset of HCM-mediated pathological remodeling of the heart.
221
222 **Genomic and transcriptomic analyses of ABE-treated mice.**
223 To determine tissue-level viral transduction and gene editing efficiency, we collected the heart,
224 lung, liver, spleen, and quadriceps muscle from saline-treated *Myh6*$^{h403/+}$ mice, and ABE-treated
225 *Myh6*$^{h403/+}$ mice at 18 weeks of age. The heart was further dissected into the right atrium, right
226 ventricle, left atrium, and left ventricle, and each chamber was separately analyzed. We conducted
227 a viral copy number assay and found similar viral transduction in all four chambers of the heart,
228 ranging from 5-9 copies of each viral half per diploid genome. The liver had the highest viral
229 transduction of the dissected tissues, with about 10 copies of each viral half per diploid genome,
230 while the spleen had the least, with about 0.2 copies of each viral half per diploid genome
231 (**Extended Data Fig. 6a**). Despite similar levels of viral copy numbers among tissues, we found
232 low levels of DNA editing in the liver, lung, spleen, and quadriceps (<0.12%) compared to DNA
233 editing in each of the heart chambers (5.5-8.0%), confirming the cardiac specificity of the cTnT
234 promoter (**Extended Data Fig. 6b**). As CMs make up only ~30% of cells [32] in the heart but are

235 the only cells to express *Myh6*, we next looked at cDNA efficiency. We found that while the left
236 atria had less correction of pathogenic transcripts compared to the ventricles, there was similar
237 editing efficiency across the four chambers (12.9-26.7%) (**Extended Data Fig. 6c**). We further
238 confirmed no changes in protein expression of key sarcomere proteins (**Extended Data Fig. 6d).**

239 To identify genomic and transcriptomic changes more deeply in CMs following base
240 editing, we isolated CM nuclei from the ventricles of saline-treated $Myh6^{WT}$ control mice, saline-
241 treated $Myh6^{h403/+}$ mice, and ABE-treated $Myh6^{h403/+}$ mice at 18 weeks of age (**Fig. 5a**). We first
242 evaluated on-target editing efficiencies following dual AAV9 ABE treatment. In ABE-treated
243 $Myh6^{h403/+}$ mice, DNA editing efficiency of the target pathogenic adenine was 32.3 ± 2.87%,
244 resulting in a 33.1 ± 9.08% reduction in pathogenic transcripts compared to $Myh6^{h403/+}$ mice (**Fig.**
245 **5b,c**), which is comparable to other *in vivo* studies using base editing [26] or RNAi-based knockdown
246 of pathogenic transcripts [33]. Furthermore, there was no detectable bystander editing in ABE-treated
247 $Myh6^{h403/+}$ mice (**Fig. 5d**). We then assessed potential off-target RNA editing via transcriptome-
248 wide RNA sequencing (RNA-seq), as ABEmax contains deaminase activity. RNA-seq analysis
249 revealed no significant increase in the average frequency of A-to-I editing in the transcriptome of
250 ABE-treated mice compared to that of saline-treated mice (**Fig. 5e**). This finding suggests that in
251 vivo treatment with our dual AAV9 ABE system does not increase RNA deamination above
252 background levels of endogenous cellular deaminase activity.

253 We next evaluated transcriptome-wide changes in ABE-treated $Myh6^{h403/+}$ mice via RNA-
254 seq. We first identified 257 differentially regulated genes between $Myh6^{WT}$ mice and $Myh6^{h403/+}$
255 mice. Heat maps showed that ABE-treated $Myh6^{h403/+}$ mice had transcriptome profiles more
256 similar to $Myh6^{WT}$ mice than to $Myh6^{h403/+}$ mice in a correction efficiency-dependent response (**Fig.**
257 **5f,** and **Extended Data Fig. 7**). Gene ontology analyses of differentially regulated genes between

Myh6$^{h403/+}$ mice and *Myh6*^{WT} mice indicated dysregulation of intercellular signaling and angiogenesis, while intercellular signaling was dysregulated between *Myh6*$^{h403/+}$ mice and ABE-treated *Myh6*$^{h403/+}$ mice (**Fig. 5g**). Additionally, expression of the prototypic hypertrophic marker *Nppa* was 2.8-fold higher in *Myh6*$^{h403/+}$ mice compared to *Myh6*^{WT} mice, while expression of *Nppa* in the ABE-treated *Myh6*$^{h403/+}$ mice was not significantly different from *Myh6*^{WT} mice (**Fig. 5h**). Taken together, these data suggest that our dual AAV9 ABE system can efficiently correct the pathogenic nucleotide in genomic DNA and prevent transcriptomic dysregulation.

Discussion

In this proof-of-concept study, we show that an adenine base editor can directly correct a common and well-studied pathogenic variant that leads to HCM, serving as a first step toward clinical translation of base editing in HCM patients. In iPSCs derived from patients with clinically diagnosed HCM, we identified the ABEmax-VRQR base editor as the optimal base editor, as it corrected the target pathogenic adenine at 98-99% efficiency in iPSCs sorted to contain all editing components with minimal bystander editing of neighboring adenines and low DNA off-target editing at tested sites within the human genome. These corrected patient-derived iPSCs, when differentiated into CMs, demonstrated normalization of contractile force~~,~~ and rescued cellular energetics compared to ~~healthy controls~~uncorrected patient-derived CMs, suggesting that correction of this pathogenic variant is sufficient to reduce the abnormalities of HCM.

To extend this work to a clinically relevant animal model, we generated a humanized mouse model of HCM. This humanized mouse model demonstrates similar HCM onset to other previously described models, but contains DNA sequence complementarity to the human allele, thus allowing testing of human-specific sgRNAs. Injection of a single dose of dual AAV9

encoding ~~for~~ ABEmax-VRQR and the h403_sgRNA in clinically relevant heterozygous postnatal *Myh6*$^{h403/+}$ mice resulted in correction of the pathogenic allele, reduction of pathogenic transcripts, and reduction in cardiac hypertrophy and histopathologic remodeling. Our study, along with the study from our colleagues [12], marks the first demonstration of efficient single nucleotide gene correction in vivo in postnatal mammalian cardiomyocytes. Future studies will seek to determine whether this rescue is sufficient to prevent HCM onset for the lifespan of the mouse.

Base editing in the *Myh6*$^{h403/h403}$ homozygous mice could double their lifespan, but ultimately could not prevent their death before weaning. This is predictable, since only the heterozygous form of the *MYH7* p.R403Q variant exists in human patients, and most likely, the homozygous form is nonviable. In mice, *Myh7* protein is partially expressed within the ventricles for the first week of life, which likely protects the heart against the pathogenic *Myh6* protein [24], as these mice die around 7 days after birth coincident with isoform switching in the ventricles. While we could achieve ~35% correction of transcripts at the highest dual AAV9 dose, the lag between healthy protein production following correction and myosin turnover and replacement of the pathogenic protein was likely too long to prevent death.

As HCM is an autosomal dominant disease, there is a strong founder effect bias in patient frequency; the initial study linking the c.1208G>A pathogenic variant to HCM was based on genetic mapping of a large French-Canadian kindred (>80 members) over five generations [34]. Nonetheless, this pathogenic variant is likely found worldwide as it was also reported in a Korean family [35]. Based on data from the Sarcomeric Human Cardiomyopathy Registry (SHaRe) [36], which performed genetic testing on HCM patients across eight different institutions in three different continents, out of all patients with identified *MYH7* gene variants, 2.4% (15/613) of them had the c.1208G>A pathogenic variant, making it the fifth most frequent pathogenic variant out of 229

304 *MYH7* variants detected. For all sarcomere gene variants identified, 0.5% (15/2763) of patients
305 had the c.1208G>A pathogenic variant. The World Bank estimates that there are 5.1 billion people
306 worldwide aged 15-64 (https://databank.worldbank.org/source/population-estimates-and-
307 projections). It is conservatively estimated that 1 in 500 people have HCM, of which 50% have a
308 known genetic cause in a sarcomere gene. From these data, we can estimate that perhaps 25,000
309 patients exist with the specific c.1208G>A p.R403Q pathogenic variant and would be amenable to
310 adenine base editing correction.

311 Although we demonstrate base editing for a single pathogenic missense variant in *MYH7*,
312 we envision that this base editing approach can be applied to the hundreds of other documented
313 missense variants in *MYH7* and to other cardiac sarcomeric proteins in which dominant-negative
314 variants lead to HCM [18]. Base editing is an ideal tool to correct the many dominant-negative
315 cardiac diseases, as gene therapy is precluded in dominant-negative diseases, and CRISPR-Cas9
316 single-cutting may edit the healthy wildtype allele, which can have deleterious effects for essential
317 genes such as *MYH7* [37]. In base editing, careful selection of a sgRNA and a base editor with
318 appropriate editing window and activity can minimize off-target binding of the sgRNA to the
319 healthy wildtype allele and minimize DNA off-target and bystander editing. As a clinical
320 treatment, we envision that while the initial base editing trials in the heart will be rigorously
321 evaluated before clinical translation, these and other initial studies will establish a pipeline for gene
322 editing of HCM. In the future, treatment of other *MYH7* pathogenic variants may then simply
323 involve changing the Cas9 variant and gRNA sequence and evaluating potential gRNA-specific
324 off-target editing for each patient's genome.

325 While our study showed that gene editing of newborn mice can prevent the onset of HCM
326 caused by the highly penetrant p.R403Q variant, some patients are genotype-positive for an HCM-

causing variant but are phenotype-negative by not demonstrating LV hypertrophy at any point in the clinical course [38]. These patients would be unlikely to need gene editing correction unless clinical HCM develops. Future studies will seek to determine whether in vivo gene editing in established HCM can either revert or limit the progression of the disease. Previous studies in a mouse [39] and cat model [40] of HCM have shown that mavacamten, a small molecule myosin inhibitor, can cause partial regression of hypertrophy in adult animals with established HCM, suggesting a potentially wide therapeutic window for other treatments such as gene editing. Use of adult animals with larger hearts could also allow testing of other delivery methods not explored in our study, such as coronary injection [41], which could then allow testing of other delivery modalities for base editors including lipid nanoparticles [42] or virus-like particles [43]. Our study also did not explore optimization in viral dosage, use of a non-targeting sgRNA as a control treatment in place of saline administration, ~~and~~ or use of other cardiogenic AAV capsid variants [44,45]. Finally, future studies will need to demonstrate correction in larger animal models that endogenously express β-myosin heavy chain predominantly within the heart, such as rabbits, cats, ~~or~~ and pigs [46], before ultimately treating HCM patients. Myosin-binding drugs that can modulate cardiac function, such as mavacamten [39], hold great promise in treating HCM; clinical trials for mavacamten have met their primary endpoints, and it was recently approved by the FDA to treat symptomatic obstructive HCM [47,48]. Nevertheless, there is a continued need for new therapeutic modalities, especially considering the on-label warning of heart failure of mavacamten [49]. Our study suggests that base editing can provide an alternative one-time treatment modality to directly and permanently correct pathogenic HCM-causing variants and prevent HCM onset, especially in cardiac genes for which no drug has been identified, or for patients with symptomatic non-

obstructive HCM, for which mavacamten did not significantly improve exercise capacity or symptoms compared to placebo [50].

Methods

Study design and approval

The objective of this study was to determine whether base editing correction of a pathogenic HCM-causing variant could prevent the onset of HCM pathological features in human CMs and a humanized mouse model. In human CMs, this was done by base editing correction of HCM patient-derived iPSCs and measuring changes in characteristic CM function. In a humanized mouse model, a dual AAV9 system was used to deliver the base editing components to CMs and changes in heart function, dimensions, and transcriptomics were measured. For all experiments, the number of replicates, type of replicates, and statistical test used ~~is~~ are reported in the figure legends. For in vitro CM experiments, data are collected from three separate differentiations, and no outliers or other data points were excluded. For in vivo experiments, male and female mice were assigned to treatment based on genotype. Echocardiographic measurements were conducted in a blinded fashion. Runt mice with reduced body weights more than 2 standard deviations from the mean were excluded. Endpoints were guided by changes in echocardiographic measurements. Animal work described in this manuscript has been approved and conducted under the oversight of the UT Southwestern Institutional Animal Care and Use Committee.

Plasmids and vector construction

The pSpCas9(BB)-2A-GFP (PX458) plasmid was a gift from Feng Zhang (Addgene plasmid #48138) [51], and was used as the primary scaffold to clone in the following base editors and SpCas9

nickases: ABE8e, a gift from David Liu (Addgene plasmid #138489) [14]; VRQR-ABEmax, a gift from David Liu (Addgene plasmid #119811) [52]; NG-ABEmax, a gift from David Liu (Addgene plasmid #124163) [52]; pCMV-T7-SpG-HF1-P2A-EGFP (RTW5000), a gift from Benjamin Kleinstiver (Addgene plasmid #139996) [15]; and pCMV-T7-SpRY-HF1-P2A-EGFP (RTW5008), a gift from Benjamin Kleinstiver (Addgene plasmid #139997) [15]. The N-terminal ABE and C-terminal ABE constructs were adapted from Cbh_v5 AAV-ABE N terminus (Addgene plasmid #137177) [53] and Cbh_v5 AAV-ABE C terminus (Addgene plasmid #137178) [53] and synthesized by Twist Bioscience. PCR amplification of select plasmids was done using PrimeStar GXL Polymerase (Takara), and cloning was done using NEBuilder HiFi DNA Assembly (NEB) into restriction enzyme-digested destination vectors.

Generation of patient-derived iPSCs and isogenic lines

Peripheral blood mononuclear cells (PBMCs) from two patients with the *MYH7* c.1208 G>A (p.R403Q) pathogenic variant were reprogrammed to iPSCs (HCM1 and ~~HCM1~~HCM2) using Sendai virus. The HCM1 line was derived from a 56-year-old female with extensive family history of HCM and nonobstructive HCM with a history of reduced left ventricular ejection fraction and low maximal oxygen uptake (VO_2 max). A biventricular pacemaker was placed for a complete heart block. The HCM2 line was derived from a 32-year-old male with a history of HCM, an implantable cardioverter-defibrillator, and a strong family history of HCM. He has a dilated left atrium but has improved VO_2 max, metabolic equivalent (METs), and no evidence of atrial fibrillation by cardiopulmonary exercise testing. These two human iPSC lines were obtained from Joseph C. Wu, MD, PhD at the Stanford Cardiovascular Institute funded by NIH R24 HL117756. PBMCs from a healthy male donor (HD) were reprogrammed to iPSCs at the UT Southwestern

Wellstone Myoediting Core using Sendai virus (CytoTune 2.0 Sendai Reprogramming Kit, ThermoFisher Scientific). To generate isogenic iPSCs containing the *MYH7* c.1208 G>A (p.R403Q) variant via homology-directed repair, HD iPSCs were nucleofected using the P3 Primary Cell 4D-Nucleofector X Kit (Lonza) with a single-stranded oligodeoxynucleotide (ssODN) template (Integrated DNA Technologies, IDT) encoding ~~for~~ the pathogenic variant, and the PX458 plasmid encoding SpCas9-P2a-EGFP and a sgRNA targeting *MYH7*. For base editing correction of HCM1 and HCM2 patient derived lines, iPSCs were nucleofected with a single plasmid encoding ~~for~~ ABEmax-VRQR-P2a-EGFP and h403_sgRNA. After 48 hours, GFP+ iPSCs were collected by fluorescence-activated cell sorting, clonally expanded, and genotyped by Sanger sequencing.

iPSC maintenance and differentiation

iPSC culture and differentiation were performed as previously described [11]. Briefly, iPSCs were cultured on Matrigel (Corning)-coated tissue culture polystyrene plates and maintained in mTeSR1 media (STEMCELL) and passaged at 70-80% confluency using Versene. iPSCs were differentiated into CMs at 70-80% confluency by treatment with CHIR99021 (Selleckchem) in RPMI supplemented with ascorbic acid (50 µg/mL) and B27 without insulin (RPMI/B27-) for 24 hrs (from day (d) 0 to d1). At d1, media was replaced with RPMI/B27-. At d3, cells were treated with RPMI/B27- supplemented with WNT-C59 (Selleckchem). At d5, media was refreshed with RPMI/B27-. From d7 onwards, iPSC-CMs were maintained in RPMI supplemented with ascorbic acid (50 µg/mL) and B27 (RPMI/B27) with media refreshed every 3-4 days. Metabolic selection of CMs was performed for 6 days starting d10 by culturing cells in RPMI without glucose and supplemented with 5 mM sodium DL-lactate and CDM3 supplement (500 µg/mL *Oryza sativa*-

418 derived recombinant human albumin, A0237, Sigma-Aldrich; and 213 µg/mL L-ascorbic acid 2-
419 phosphate, Sigma-Aldrich). To induce their maturation, iPSC-CMs were maintained in RPMI
420 without glucose supplemented with B27, 50 µmol palmitic acid, 100 µmol oleic acid, 10 mmol
421 galactose, and 1 mmol glutamine (Sigma-Aldrich) [54,55]. All CM functional studies were done at
422 d40-50.
423

424 **Plasmid transfection and editing efficiency analysis**

425 iPSCs were seeded on a 48-well plate 24 h before transfection. At ~20% confluency, cells were
426 transiently transfected with 0.5 µg of plasmid encoding ~~for~~ a base editor and the h403_sgRNA
427 using 1 µL of Lipofectamine Stem Transfection Reagent (ThermoFisher) per well. Following 48
428 h post-transfection, cells were lysed in Direct PCR Lysis Reagent (Cell) (Viagen). PCR
429 amplification of target sites was done using PrimeStar GXL Polymerase (Takara), and PCR
430 cleanup was done using ExoSap-IT Express (ThermoFisher) before Sanger sequencing.
431 Chromatograms were analyzed using EditR to determine base editing efficiencies [56].
432

433 **Contractility analyses of iPSC-CMs**

434 iPSC-CMs were plated at single-cell density on flexible polydimethylsiloxane (PDMS) 527
435 substrates (Young's modulus = 5 kPa) prepared according to a previously established protocol [57].
436 Recordings of contracting iPSC-CMs were captured at 37 °C using a Nikon A1R+ confocal system
437 at 59 frames per second in resonance scanning mode. Contractile force generation of iPSC-CMs
438 was quantified using a previously established method. In brief, recordings were analyzed using
439 Fiji to measure maximum and minimum cell lengths, and cell widths during contraction. A
440 previously published customized MATLAB code was used to calculate peak systolic forces [58].

441

442 **Extracellular flux analyses of iPSC-CMs**

443 iPSC-CMs were plated at 40,000 cells per well in Seahorse XFe96 V3 PS Cell Culture Microplates
444 (Agilent) coated with Matrigel. One-week post-plating, cells were washed three times with
445 prewarmed assay media (pyruvate-free DMEM (Sigma D5030) supplemented with 2 mM L-
446 glutamine, 1 mM sodium pyruvate, and 10 mM glucose, pH 7.4) and incubated at 37 °C for 60
447 min in a non-CO_2 incubator. Oxygen consumption rate (OCR) was measured in a Seahorse XFe96
448 instrument using consecutive cycles of 2 mins of measurement, 10 seconds of waiting, and 3
449 minutes of mixing. Mitochondrial stress testing was performed by injecting oligomycin (final
450 concentration 2 μM), CCCP (final concentration 1 μM), and antimycin A (final concentration 1
451 μM) at indicated time intervals. Data were analyzed using the WAVE software (Agilent).

452

453 **Immunofluorescence staining**

454 iPSC-CMs were plated on glass surfaces and fixed with 4% paraformaldehyde for 10 min,
455 followed by blocking with 5% goat serum/0.1% Tween-20 (Sigma-Aldrich) for 1 hr. Primary and
456 secondary antibodies were diluted in blocking buffer and added to cells for 2 hr and 1 hr,
457 respectively. Nuclei were counterstained using DAPI. Antibodies used included rabbit anti-
458 troponin-I (H-170 sc-15368, Santa Cruz Biotechnology, 1:200), and fluorescein-conjugated
459 donkey anti-rabbit IgG (711-095-152, Jackson ImmunoResearch, 1:50).

460

461 **Off-target analyses**

462 Candidate off-target sites were identified with CRISPOR, and the top 8 sites by cutting frequency
463 determination (CFD) score, for which PCR products were successfully obtained, were selected

464 [19,59]. Genomic DNA was isolated using a DNeasy Blood & Tissue Kit (Qiagen) from HCM1 and
465 HCM2 cell lines that had been nucleofected with plasmids encoding ~~for~~ ABEmax- VRQR-P2a-
466 EGFP and h403_sgRNA and sorted for GFP+ cells. Target sites were PCR amplified using
467 PrimeStar GXL Polymerase (Takara), and a second round of PCR was used to add Illumina flow
468 cell binding sequences and barcodes. PCR products were purified with AMPure XP Beads
469 (Beckman Coulter), analyzed for integrity on a 2200 TapeStation System (Agilent), and quantified
470 by QuBit dsDNA high-sensitivity assay (Invitrogen) before pooling and loading onto an Illumina
471 MiSeq. Following demultiplexing, resulting reads were analyzed with CRISPResso2 for editing
472 frequency [60].
473
474 **Generation of adeno-associated viruses**
475 Recombinant AAV9 (rAAV9) viruses were made at the University of Michigan Vector Core using
476 ultracentrifugation through an iodixanol gradient. rAAV9s were washed 3 times with PBS using
477 Amicon Ultra Centrifugal Filter Units (Millipore) and resuspended in PBS + 0.001% Pluronic F68.
478 Titers were assessed by qPCR. rAAV9 was stored in 25 µL aliquots at -80 °C.
479
480 **Mice**
481 Mice were housed in a barrier facility with a 12-hour:12-hour light:dark cycle and maintained on
482 standard chow (2916 Teklad Global). The humanized *Myh6*$^{h403/+}$ pathogenic variant was
483 introduced via microinjection of zygotes with Cas9 mRNA (50 ng/µL) (TriLink Biotechnologies),
484 a sgRNA (20 ng/µL) (IDT), and a ssODN donor template (15 ng/µL) (IDT) following a modified
485 protocol [61]. Genotyping was performed using a custom TaqMan SNP Genotyping Assay (Assay
486 ID: ANPRZE6) (ThermoFisher). To accelerate the onset of HCM, mice were treated with a custom

487 chow (2916 Teklad Global base) containing Cyclosporine A (Alfa Aesar) at 1 g/kg and blue food
488 dye at 0.2 g/kg. For injections, mice were genotyped at P0 and received either saline or a AAV9
489 dose via a single 40 μL bolus using a 31G insulin syringe through the diaphragm by a subxiphoid
490 approach into the inferior mediastinum, avoiding the heart and the lung.
491

492 **Transthoracic echocardiography**

493 Cardiac function on conscious mice was evaluated by two-dimensional transthoracic
494 echocardiography using a VisualSonics Vevo2100 imaging system. M-mode tracings were used
495 to measure LV anterior wall thickness at diastole (LVAW;d), LV posterior wall thickness at
496 diastole (LVPW;d), and LV internal diameter at end diastole (LVIDd) and end systole (LVIDs).
497 FS was calculated according to the following formula: FS (%) = [(LVIDd – LVIDs)/LVIDd] ×
498 100. EF was calculated according to the following formula: EF (%) = [(LVEDV –
499 LVESV)/LVEDV] x 100. All measurements were performed by an experienced operator blinded
500 to the study.
501

502 **Histology**

503 Mouse hearts were dissected out and submerged in PBS with cardioplegic 0.2M KCl for 5 minutes
504 before fixation in 4% paraformaldehyde in PBS overnight, followed by dehydration in 70%
505 ethanol and paraffin embedding. Serial transverse cross-sections at 500 μm intervals were cut and
506 mounted on slides, followed by H&E staining, Picrosirius Red, or Masson's Trichrome staining.
507 Images were captured on a BZ-X800 all-in-one microscope (Keyence) at 10x or 40x
508 magnification. Analyses were performed with Fiji and Adobe Photoshop.
509

510 **Viral copy number (VCN) assay**

511 Genomic DNA was isolated from mouse tissue using the DNeasy Blood & Tissue Kit (Qiagen).
512 AAV VCN was determined by quantitative PCR (qPCR) using custom-designed primers and
513 Taqman probes (IDT) (**Supplementary Table 1.**) and the Applied Biosystems TaqMan Fast
514 Advanced Master Mix (Applied Biosystems). The primers and probes anneal to the N-terminal
515 and C-terminal Cas9 genes. A copy number standard curve of the AAV plasmids used for
516 packaging was used to determine copy number for each cycle threshold. The 18S ribosomal RNA
517 gene was used as a reference to calculate genomic DNA quantity.

518

519 **Cardiac myofibril isolation and analysis**

520 Cardiac myofibrils were isolated from hearts using a previously reported protocol, with minor
521 modifications [62]. Collected hearts were homogenized using CK28-R hard tissue homogenizing
522 tubes in the Percellys homogenizer (Bertin Instruments) on the hard tissue setting. Following
523 myofibril isolation, protein amounts were quantified by Pierce BCA Protein Assay
524 (ThermoFisher). For each sample, 10 μg protein was run on a 4-20% polyacrylamide gel, then
525 stained with Coomassie G-250.

526

527 **CM nuclei isolation**

528 For each nuclear sample, ventricular heart tissue was isolated. CM nuclei were isolated as
529 previously described [63]. Isolated nuclei were immediately used for downstream processing. RNA
530 was isolated from nuclei using the RNeasy Micro Kit (Qiagen). For qPCR and cDNA HTS, RNA
531 was reverse transcribed using iScript cDNA Synthesis Kit (Bio-Rad). For DNA sequencing, nuclei
532 were lysed in Direct PCR Lysis Reagent (Cell) (Viagen).

533

534 **Mouse DNA and cDNA sequencing and analysis**

535 On-target DNA and cDNA sites were PCR amplified using PrimeStar GXL Polymerase (Takara),
536 and a second round of PCR was used to add Illumina flow cell binding sequences and barcodes.
537 PCR products were purified with AMPure XP Beads (Beckman Coulter), analyzed for integrity on
538 a 2200 TapeStation System (Agilent), and quantified by QuBit dsDNA high-sensitivity assay
539 (Invitrogen) before pooling and loading onto an Illumina MiSeq. Following demultiplexing,
540 resulting reads were analyzed with CRISPResso2 for editing frequency [60].

541

542 **RNA-seq library preparation, sequencing, and analysis**

543 RNA-seq libraries were generated using the SMARTer Stranded Total RNA-Seq Kit v2-Pico Input
544 Mammalian kit (Takara), containing Illumina sequencing adapters. Libraries were visualized on a
545 2200 TapeStation System (Agilent) and quantified by QuBit dsDNA high-sensitivity assay
546 (Invitrogen) before pooling and loading onto an Illumina NextSeq 500. FastQC tool (Version
547 0.11.8) was used for quality control of RNA-seq data to determine low quality or adapt~~eo~~r portions
548 of the reads for trimming. Read trimming was performed using Trimmomatic (Version 0.39) and
549 strandness was determined using RSeQC (Version 4.0.0) and then reads were aligned to the mm10
550 reference genome using HiSAT2 (Version 2.1.0) with default settings and -rna-strandness R.
551 Aligned reads were counted using featureCounts (Version 1.6.2). Differential gene expression
552 analysis was performed using R package DESeq (Version 1.38.0). Genes with fold-change >2 and
553 p-value <0.01 were designated as DEGs between sample group comparisons. To calculate the
554 average percentage of A-to-I editing amongst adenosines sequenced in transcriptome-wide
555 sequencing analysis, we adopted a previous strategy [9]. In brief, REDItools2 was used to quantify

556 the percentage editing in each sample. Nucleotides except adenosines were removed and remaining
557 adenosines with read coverage less than 10 or read quality score below 25 were also filtered to
558 avoid errors due to low sampling or low sequencing quality. We then calculated the number of A-
559 to-I conversion in each sample and divided this by the total number of adenosines in our dataset
560 after filtering to get the percentage of A-to-I editing in the transcriptome.
561

562 **Quantitative real-time PCR analysis**

563 qPCR reactions were assembled using Applied Biosystems TaqMan Fast Advanced Master Mix
564 (Applied Biosystems). Assays were performed using Applied Biosystems QuantStudio 5 Real-
565 Time PCR System (Applied Biosystems). Expression values were normalized to *18S* mRNA and
566 represented as fold change.
567

568 **Statistics**

569 All data are presented as means ± s.e.m. or means ± s.d. as indicated. Unpaired two-tailed Student's
570 t tests were performed for comparison between the respective two groups as indicated in the
571 figures. Kaplan-Meier analysis and Log-rank (Mantel-Cox) test were used to evaluate the
572 difference in survival between different genotypes. Data analyses were performed with statistical
573 software (GraphPad Prism Software). *P* values less than 0.05 were considered statistically
574 significant.
575

576 **Data and materials availability:** All data needed to evaluate the conclusions in the paper are
577 present in the paper, extended data, and supplementary materials. Raw and analyzed RNA-
578 sequencing data generated during this study are available in the Gene Expression Omnibus

579 (GEO) repository (http://www.ncbi.nlm.nih.gov/geo/) and are accessible through GEO series
580 accession number GSE201755.
581
582 **Code availability:** The MATLAB code used to perform contractile force measurements of
583 iPSC-CMs has been deposited to GitHub: https://github.com/DarisaLLC/Cardio.
584

585 **Extended Data**

586 Extended Data Fig. 1-7.

587 **Supplementary Information**

588 Supplementary Fig. 1-2.

589 Supplementary Table 1.

590 **References and Notes**

591 1. Maron, B.J. Clinical Course and Management of Hypertrophic Cardiomyopathy. *N Engl*
592 *J Med* **379**, 655-668 (2018).
593 2. Semsarian, C., Ingles, J., Maron, M.S. & Maron, B.J. New perspectives on the prevalence
594 of hypertrophic cardiomyopathy. *J Am Coll Cardiol* **65**, 1249-1254 (2015).
595 3. Trivedi, D.V., Adhikari, A.S., Sarkar, S.S., Ruppel, K.M. & Spudich, J.A. Hypertrophic
596 cardiomyopathy and the myosin mesa: viewing an old disease in a new light. *Biophys Rev*
597 **10**, 27-48 (2018).
598 4. Geisterfer-Lowrance, A.A.*, et al.* A molecular basis for familial hypertrophic
599 cardiomyopathy: a beta cardiac myosin heavy chain gene missense mutation. *Cell* **62**,
600 999-1006 (1990).
601 5. Tyska, M.J.*, et al.* Single-molecule mechanics of R403Q cardiac myosin isolated from
602 the mouse model of familial hypertrophic cardiomyopathy. *Circ Res* **86**, 737-744 (2000).
603 6. Sarkar, S.S.*, et al.* The hypertrophic cardiomyopathy mutations R403Q and R663H
604 increase the number of myosin heads available to interact with actin. *Sci Adv* **6**, eaax0069
605 (2020).
606 7. Gaudelli, N.M.*, et al.* Programmable base editing of A*T to G*C in genomic DNA
607 without DNA cleavage. *Nature* **551**, 464-471 (2017).

608 8. Komor, A.C., Kim, Y.B., Packer, M.S., Zuris, J.A. & Liu, D.R. Programmable editing of
609 a target base in genomic DNA without double-stranded DNA cleavage. *Nature* **533**, 420-
610 424 (2016).
611 9. Koblan, L.W.*, et al.* In vivo base editing rescues Hutchinson-Gilford progeria syndrome
612 in mice. *Nature* **589**, 608-614 (2021).
613 10. Suh, S.*, et al.* Restoration of visual function in adult mice with an inherited retinal disease
614 via adenine base editing. *Nat Biomed Eng* **5**, 169-178 (2021).
615 11. Chemello, F.*, et al.* Precise correction of Duchenne muscular dystrophy exon deletion
616 mutations by base and prime editing. *Sci Adv* **7**(2021).
617 12. Reichart, D.*, et al.* Efficient in vivo Genome Editing Prevents Hypertrophic
618 Cardiomyopathy in Mice. *Nature Medicine* (2022).
619 13. Koblan, L.W.*, et al.* Improving cytidine and adenine base editors by expression
620 optimization and ancestral reconstruction. *Nat Biotechnol* **36**, 843-846 (2018).
621 14. Richter, M.F.*, et al.* Phage-assisted evolution of an adenine base editor with improved
622 Cas domain compatibility and activity. *Nat Biotechnol* **38**, 883-891 (2020).
623 15. Walton, R.T., Christie, K.A., Whittaker, M.N. & Kleinstiver, B.P. Unconstrained genome
624 targeting with near-PAMless engineered CRISPR-Cas9 variants. *Science* **368**, 290-296
625 (2020).
626 16. Nishimasu, H.*, et al.* Engineered CRISPR-Cas9 nuclease with expanded targeting space.
627 *Science* **361**, 1259-1262 (2018).
628 17. Kleinstiver, B.P.*, et al.* High-fidelity CRISPR-Cas9 nucleases with no detectable
629 genome-wide off-target effects. *Nature* **529**, 490-495 (2016).
630 18. Marian, A.J. & Braunwald, E. Hypertrophic Cardiomyopathy: Genetics, Pathogenesis,
631 Clinical Manifestations, Diagnosis, and Therapy. *Circ Res* **121**, 749-770 (2017).
632 19. Concordet, J.P. & Haeussler, M. CRISPOR: intuitive guide selection for CRISPR/Cas9
633 genome editing experiments and screens. *Nucleic Acids Res* **46**, W242-W245 (2018).
634 20. Pua, C.J.*, et al.* Genetic Studies of Hypertrophic Cardiomyopathy in Singaporeans
635 Identify Variants in TNNI3 and TNNT2 That Are Common in Chinese Patients. *Circ*
636 *Genom Precis Med* **13**, 424-434 (2020).
637 21. Toepfer, C.N.*, et al.* Myosin Sequestration Regulates Sarcomere Function,
638 Cardiomyocyte Energetics, and Metabolism, Informing the Pathogenesis of Hypertrophic
639 Cardiomyopathy. *Circulation* **141**, 828-842 (2020).
640 22. Cohn, R.*, et al.* A Contraction Stress Model of Hypertrophic Cardiomyopathy due to
641 Sarcomere Mutations. *Stem Cell Reports* **12**, 71-83 (2019).
642 23. Vakrou, S. & Abraham, M.R. Hypertrophic cardiomyopathy: a heart in need of an energy
643 bar? *Front Physiol* **5**, 309 (2014).
644 24. Lyons, G.E., Schiaffino, S., Sassoon, D., Barton, P. & Buckingham, M. Developmental
645 regulation of myosin gene expression in mouse cardiac muscle. *J Cell Biol* **111**, 2427-
646 2436 (1990).
647 25. Geisterfer-Lowrance, A.A.*, et al.* A mouse model of familial hypertrophic
648 cardiomyopathy. *Science* **272**, 731-734 (1996).
649 26. Ma, S.*, et al.* Efficient Correction of a Hypertrophic Cardiomyopathy Mutation by
650 ABEmax-NG. *Circ Res* **129**, 895-908 (2021).
651 27. Ishikawa, K., Weber, T. & Hajjar, R.J. Human Cardiac Gene Therapy. *Circ Res* **123**, 601-
652 613 (2018).

653 28. Zettler, J., Schutz, V. & Mootz, H.D. The naturally split Npu DnaE intein exhibits an
654 extraordinarily high rate in the protein trans-splicing reaction. *FEBS Lett* **583**, 909-914
655 (2009).
656 29. Prasad, K.M., Xu, Y., Yang, Z., Acton, S.T. & French, B.A. Robust cardiomyocyte-
657 specific gene expression following systemic injection of AAV: in vivo gene delivery
658 follows a Poisson distribution. *Gene Ther* **18**, 43-52 (2011).
659 30. Cellular, T., and Gene Therapies Advisory Committee (CTGTAC) Meeting #70. Toxicity
660 Risks of Adeno-associated Virus (AAV) Vectors for Gene Therapy. (ed. (FDA),
661 F.a.D.A.) (FDA-2021-N-0651, 2021).
662 31. Teekakirikul, P.*, et al.* Cardiac fibrosis in mice with hypertrophic cardiomyopathy is
663 mediated by non-myocyte proliferation and requires Tgf-beta. *J Clin Invest* **120**, 3520-
664 3529 (2010).
665 32. Pinto, A.R.*, et al.* Revisiting Cardiac Cellular Composition. *Circ Res* **118**, 400-409
666 (2016).
667 33. Jiang, J., Wakimoto, H., Seidman, J.G. & Seidman, C.E. Allele-specific silencing of
668 mutant Myh6 transcripts in mice suppresses hypertrophic cardiomyopathy. *Science* **342**,
669 111-114 (2013).
670 34. Pare, J.A., Fraser, R.G., Pirozynski, W.J., Shanks, J.A. & Stubington, D. Hereditary
671 cardiovascular dysplasia. A form of familial cardiomyopathy. *Am J Med* **31**, 37-62
672 (1961).
673 35. Fananapazir, L. & Epstein, N.D. Genotype-phenotype correlations in hypertrophic
674 cardiomyopathy. Insights provided by comparisons of kindreds with distinct and identical
675 beta-myosin heavy chain gene mutations. *Circulation* **89**, 22-32 (1994).
676 36. Ho, C.Y.*, et al.* Genotype and Lifetime Burden of Disease in Hypertrophic
677 Cardiomyopathy: Insights from the Sarcomeric Human Cardiomyopathy Registry
678 (SHaRe). *Circulation* **138**, 1387-1398 (2018).
679 37. Carroll, K.J.*, et al.* A mouse model for adult cardiac-specific gene deletion with
680 CRISPR/Cas9. *Proc Natl Acad Sci U S A* **113**, 338-343 (2016).
681 38. Maron, B.J., Yeates, L. & Semsarian, C. Clinical challenges of genotype positive (+)-
682 phenotype negative (-) family members in hypertrophic cardiomyopathy. *Am J Cardiol*
683 **107**, 604-608 (2011).
684 39. Green, E.M.*, et al.* A small-molecule inhibitor of sarcomere contractility suppresses
685 hypertrophic cardiomyopathy in mice. *Science* **351**, 617-621 (2016).
686 40. Stern, J.A.*, et al.* A Small Molecule Inhibitor of Sarcomere Contractility Acutely
687 Relieves Left Ventricular Outflow Tract Obstruction in Feline Hypertrophic
688 Cardiomyopathy. *PLoS One* **11**, e0168407 (2016).
689 41. Ladage, D., Ishikawa, K., Tilemann, L., Muller-Ehmsen, J. & Kawase, Y. Percutaneous
690 methods of vector delivery in preclinical models. *Gene Ther* **19**, 637-641 (2012).
691 42. Cheng, Q.*, et al.* Selective organ targeting (SORT) nanoparticles for tissue-specific
692 mRNA delivery and CRISPR-Cas gene editing. *Nat Nanotechnol* **15**, 313-320 (2020).
693 43. Banskota, S.*, et al.* Engineered virus-like particles for efficient in vivo delivery of
694 therapeutic proteins. *Cell* **185**, 250-265 e216 (2022).
695 44. Tabebordbar, M.*, et al.* Directed evolution of a family of AAV capsid variants enabling
696 potent muscle-directed gene delivery across species. *Cell* **184**, 4919-4938 e4922 (2021).
697 45. Weinmann, J.*, et al.* Identification of a myotropic AAV by massively parallel in vivo
698 evaluation of barcoded capsid variants. *Nat Commun* **11**, 5432 (2020).

46. Lompre, A.M., *et al.* Species- and age-dependent changes in the relative amounts of cardiac myosin isoenzymes in mammals. *Dev Biol* **84**, 286-290 (1981).
47. Desai, M.Y., *et al.* Study design and rationale of VALOR-HCM: evaluation of mavacamten in adults with symptomatic obstructive hypertrophic cardiomyopathy who are eligible for septal reduction therapy. *Am Heart J* **239**, 80-89 (2021).
48. Saberi, S., *et al.* Mavacamten Favorably Impacts Cardiac Structure in Obstructive Hypertrophic Cardiomyopathy: EXPLORER-HCM Cardiac Magnetic Resonance Substudy Analysis. *Circulation* **143**, 606-608 (2021).
49. FDA, U. CAMZYOS (mavacamten) capsules for oral use. (2022).
50. Ho, C.Y., *et al.* Evaluation of Mavacamten in Symptomatic Patients With Nonobstructive Hypertrophic Cardiomyopathy. *J Am Coll Cardiol* **75**, 2649-2660 (2020).
51. Ran, F.A., *et al.* Genome engineering using the CRISPR-Cas9 system. *Nat Protoc* **8**, 2281-2308 (2013).
52. Huang, T.P., *et al.* Circularly permuted and PAM-modified Cas9 variants broaden the targeting scope of base editors. *Nat Biotechnol* **37**, 626-631 (2019).
53. Levy, J.M., *et al.* Cytosine and adenine base editing of the brain, liver, retina, heart and skeletal muscle of mice via adeno-associated viruses. *Nat Biomed Eng* **4**, 97-110 (2020).
54. Burridge, P.W., *et al.* Chemically defined generation of human cardiomyocytes. *Nat Methods* **11**, 855-860 (2014).
55. Correia, C., *et al.* Distinct carbon sources affect structural and functional maturation of cardiomyocytes derived from human pluripotent stem cells. *Sci Rep* **7**, 8590 (2017).
56. Kluesner, M.G., *et al.* EditR: A Method to Quantify Base Editing from Sanger Sequencing. *CRISPR J* **1**, 239-250 (2018).
57. Atmanli, A., *et al.* Cardiac Myoediting Attenuates Cardiac Abnormalities in Human and Mouse Models of Duchenne Muscular Dystrophy. *Circ Res* **129**, 602-616 (2021).
58. Kijlstra, J.D., *et al.* Integrated Analysis of Contractile Kinetics, Force Generation, and Electrical Activity in Single Human Stem Cell-Derived Cardiomyocytes. *Stem Cell Reports* **5**, 1226-1238 (2015).
59. Doench, J.G., *et al.* Optimized sgRNA design to maximize activity and minimize off-target effects of CRISPR-Cas9. *Nat Biotechnol* **34**, 184-191 (2016).
60. Clement, K., *et al.* CRISPResso2 provides accurate and rapid genome editing sequence analysis. *Nat Biotechnol* **37**, 224-226 (2019).
61. Miura, H., Quadros, R.M., Gurumurthy, C.B. & Ohtsuka, M. Easi-CRISPR for creating knock-in and conditional knockout mouse models using long ssDNA donors. *Nat Protoc* **13**, 195-215 (2018).
62. Creed, H.A. & Tong, C.W. Preparation and Identification of Cardiac Myofibrils from Whole Heart Samples. *Methods Mol Biol* **2319**, 15-24 (2021).
63. Cui, M. & Olson, E.N. Protocol for Single-Nucleus Transcriptomics of Diploid and Tetraploid Cardiomyocytes in Murine Hearts. *STAR Protoc* **1**, 100049 (2020).

Acknowledgments: We thank the members of the E.N.O laboratory for helpful discussions; Dr. J.C. Wu and the Stanford Cardiovascular Institute for providing the HCM patient-derived iPSCs; Drs. C. Seidman and H. Wakimoto for suggestions on intrathoracic AAV9 delivery; Drs. T.

742 Lanigan, H. Kopera, and R. Agate from the University of Michigan Vector Core for rAAV9
743 production; C. Llamas, and Dr. P. Mishra from the Children's Medical Center Research Institute
744 (CRI) for help with Seahorse assays; J. Cabrera and Dr. S. Vargas for graphics; Dr. D. Martin
745 from Envigo for custom chow consultation; Drs. J. Xu and Y.J. Kim from the CRI for
746 performing the Illumina NextSeq sequencing; C. Rodriguez-Caycedo for assistance with iPSCs;
747 the UT Southwestern McDermott Center Sanger Sequencing Core; the UT Southwestern
748 McDermott Center Next Generation Sequencing Core; the UT Southwestern Flow Cytometry
749 Core; and J. Shelton from the Molecular Histopathology Core for help with histology. This work
750 was supported by grants from the National Institutes of Health (HL-130253, HD-087351, and
751 HL-157281 to E.N.O.; F30HL163915 to A.C.C.), the American Heart Association (907611 to
752 A.C.C.), the Foundation Leducq Transatlantic Networks of Excellence in Cardiovascular
753 Research, and the Robert A. Welch Foundation (grant 1-0025 to E.N.O.).

754

755 **Author contributions:**

756 A.C.C., R.B.D., and E.N.O. conceived of the project and designed the experiments. A.C.C., F.C.,
757 H.L., and A.A. conducted in vitro iPSC-CM experiments. A.C.C., M.C., F.C., H.L., and Y.Z.
758 conducted in vivo experiments. W.T. performed mouse echocardiography. J.M. performed
759 mouse zygote injections. K.C., A.C.C., and L.X. performed bioinformatics analysis. A.C.C.,
760 N.L., R.B.D., and E.N.O. wrote the manuscript.

761

762 **Competing interests:** E.N.O. is a consultant for Vertex Pharmaceuticals and Tenaya
763 Therapeutics. The other authors declare that they have no competing interests.

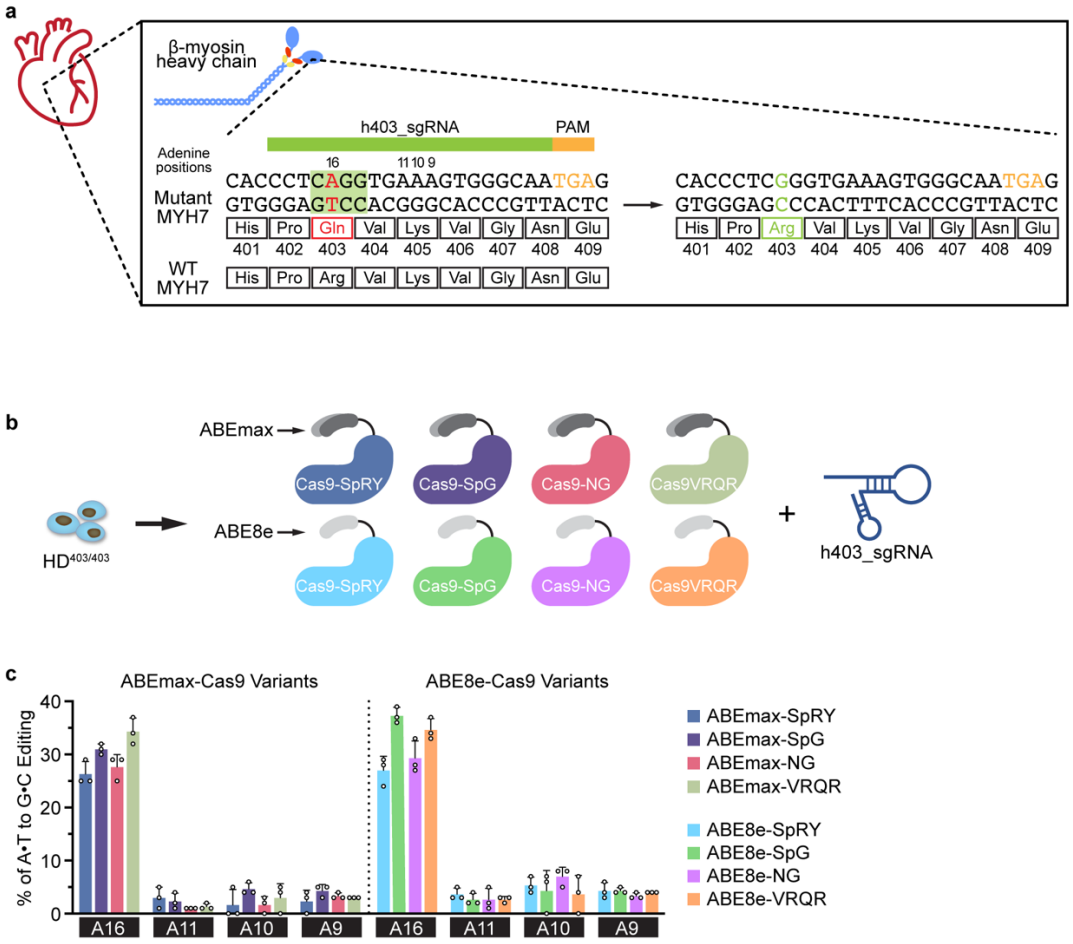

764

765 **Fig. 1: In vitro optimization of ABE system to correct a pathogenic *MYH7* variant. a,** A
766 candidate sgRNA, h403_sgRNA, for base editing to correct the *MYH7* c.1208G>A (p.R403Q)
767 missense variant. Base editing could convert the neutrally charged glutamine pathogenic variant
768 back to a positively charged arginine, restoring proper function of the myosin head. **b,** Eight
769 candidate base editor variants were screened for their efficiencies in correcting the pathogenic
770 adenine to a guanine using the candidate h403_sgRNA within a homozygous *MYH7* c.1208G>A
771 iPSC line ($HD^{403/403}$). **c,** DNA editing efficiency of all adenines within the target protospacer in
772 $HD^{403/403}$ iPSCs 72 h post-transfection with candidate base editors. Data are mean ± s.d. across
773 three technical replicates. Numbering is with the first base 5' of the PAM as 1; target pathogenic
774 adenine is position A16.

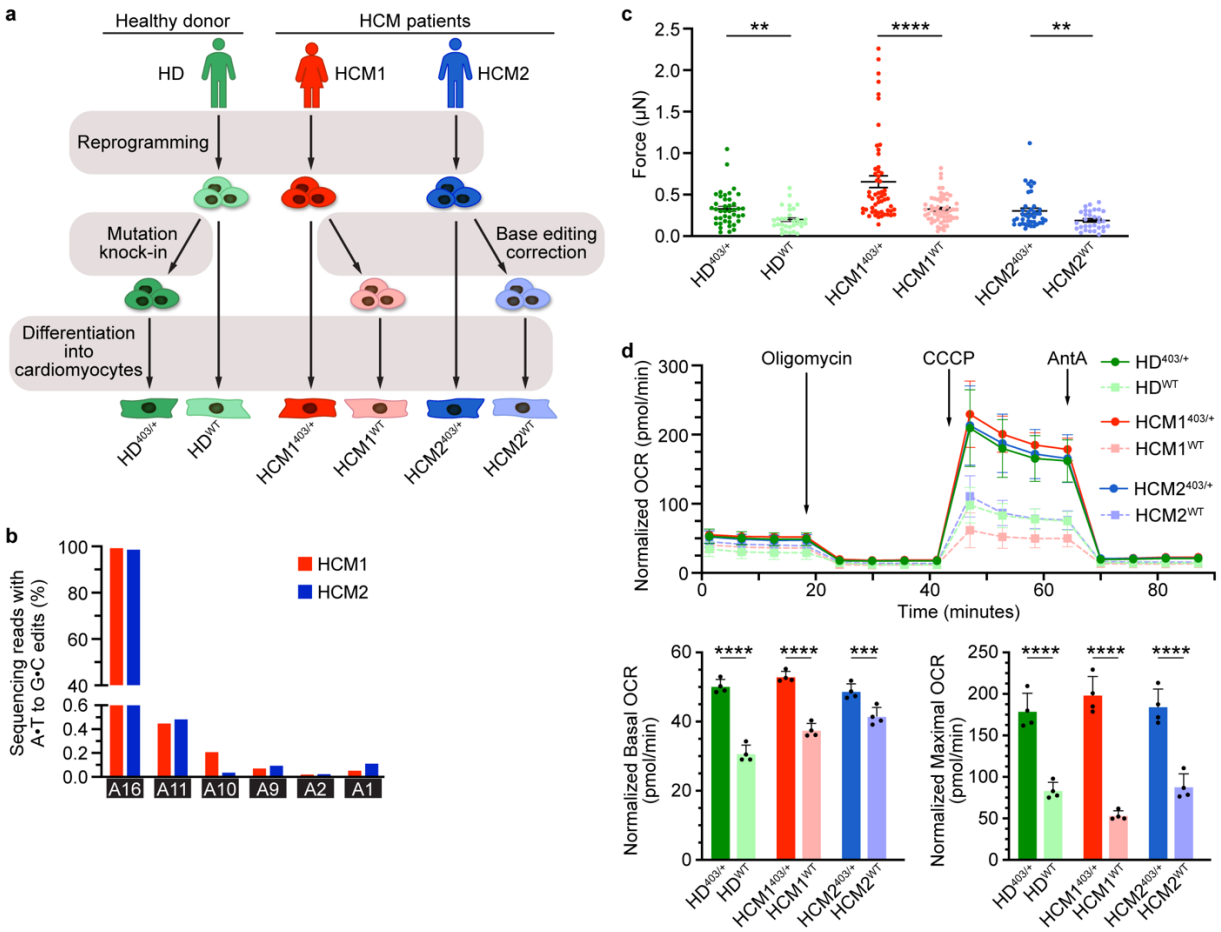

Fig. 2: Analyses of HCM patient-derived iPSC-CM function upon base editing correction. a, Workflow for reprogramming iPSCs from a healthy donor (HD) and two HCM patients (HCM1 and HCM2), followed by pathogenic variant knock-in for the HD line, and base editing correction for the HCM1 and HCM2 lines. Isogenic clonal lines were then isolated and differentiated into CMs for downstream analyses of iPSC-CM function. **b,** ~~Deep~~ High throughput sequencing (HTS) to measure editing for all adenines within the on-target protospacer. Target pathogenic adenine is A16. ~~Deep sequencing~~HTS was performed for ABE-treated ~~*MYH7*$^{403/+}$~~ HCM1$^{403/+}$, and ~~*MYH7*$^{403/+}$~~ HCM2$^{403/+}$ iPSCs. **c,** Quantification of peak systolic force of ~~*MYH7*$^{403/+}$ and *MYH7*^{WT}~~ iPSC-CMs ~~from HD, HCM1, and HCM2 patients~~for indicated cell lines. (n=31-57 for each genotype) Data are mean ± s.e.m. across three separate differentiations. **d,** Oxygen consumption rate (OCR) as a

786 function of time in indicated cell lines following exposure to the electron transport chain complex
787 inhibitors, oligomycin, carbonyl cyanide *m*-chlorophenyl hydrazone (CCCP), and Antimycin A
788 (AntA) (top), and mean and distribution of values across four timepoints for basal OCR (bottom
789 left) and maximal OCR (bottom right) for indicated cell lines. Data are mean ± s.d. across three
790 separate differentiations. Each data point is from 14-16 Seahorse assay wells. $^{**}P < 0.01$, $^{***}P <$
791 0.001, $^{****}P < 0.0001$ by Student's unpaired two-sided t-test.

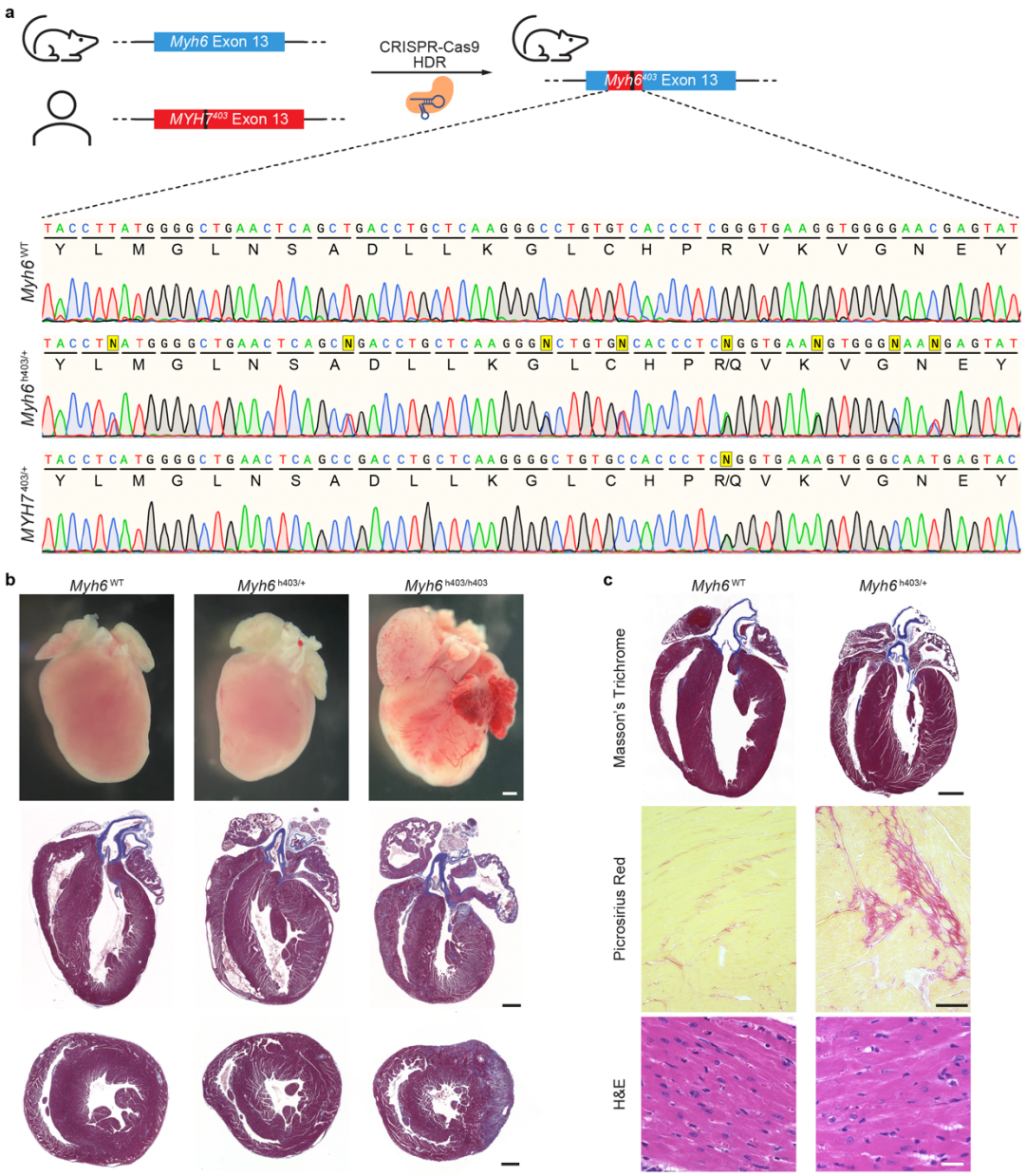

Fig. 3: Generation of a humanized HCM mouse model. **a,** A humanized HCM mouse model generated was by replacing part of the native murine *Myh6* genomic sequence with the human *MYH7* sequence containing the p.R403Q variant via CRISPR-Cas9 homology-directed repair (HDR). Sanger sequencing chromatograms show the native *Myh6*^{WT} sequence (top), the humanized *Myh6*$^{h403/+}$ mouse model sequence (middle), and a human HCM patient-derived iPSC line sequence (bottom). Yellow squares indicate knocked-in SNPs; Sanger sequencing shows

799 double nucleotide peaks for SNPs. **b,** Gross histology (top), and Masson's trichrome staining of
800 coronal (4-chamber) (middle) and transverse (bottom) sections of the humanized mouse model for
801 the wildtype (left), heterozygous (middle), and homozygous (right) genotypes at postnatal day 8.
802 Scale bar, 1 mm. **c,** Masson's trichrome, Picrosirius red, and hematoxylin & eosin staining of heart
803 sections of the humanized mouse model for the wildtype (left) and heterozygous (right) genotypes
804 at 9 months of age. Scale bar, 1 mm for 10x images top, 100 μm for 10x images middle, 25 μm
805 for 40x images bottom.
806

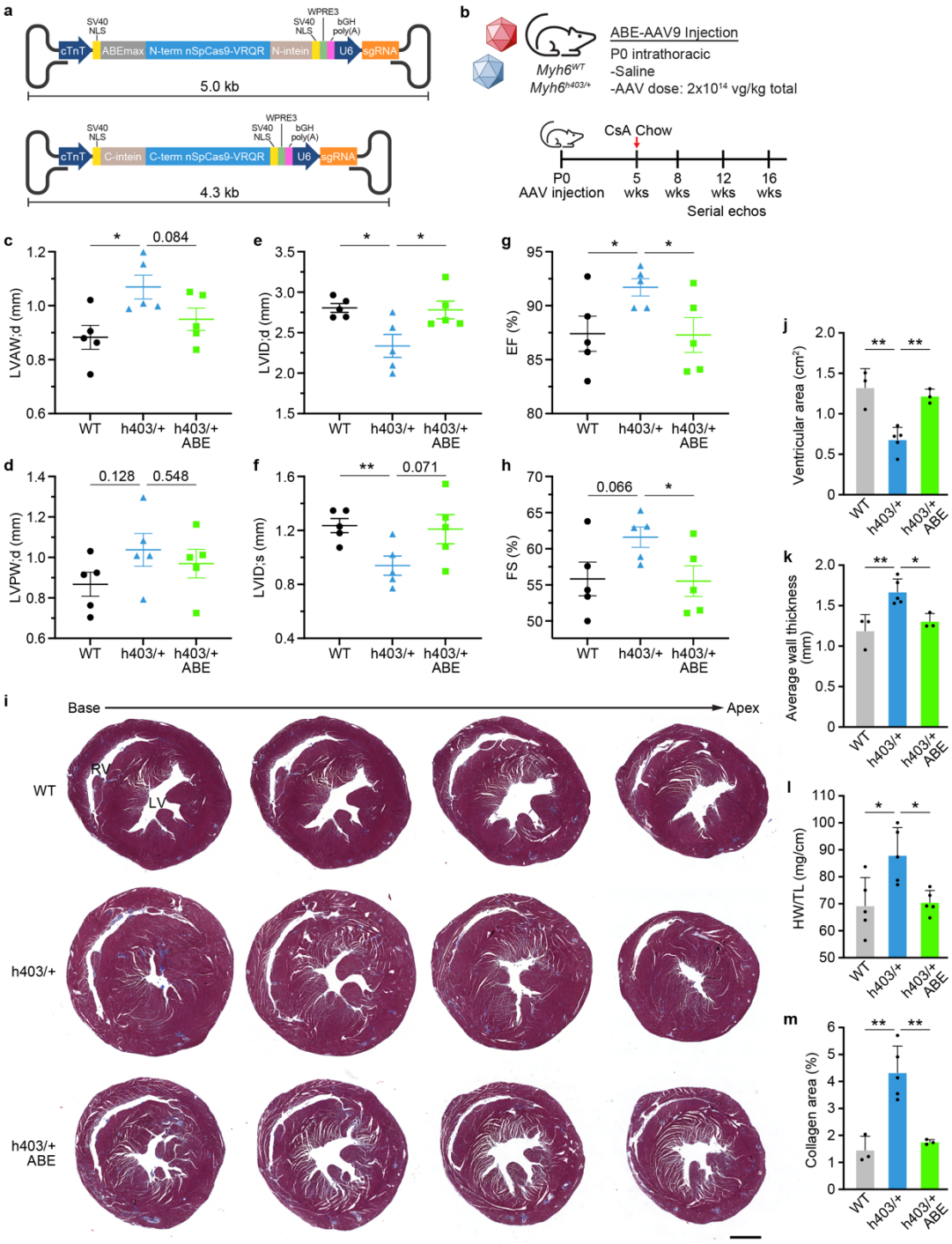

807

808 **Fig. 4: Prevention of HCM by dual AAV9 ABE editing of *Myh6*$^{h403/+}$ mice**. **a,** Schematic of
809 dual AAV9 ABE system encoding ABEmax-VRQR base editor halves and h403_sgRNA to target
810 the human *MYH7* p.R403Q variant. **b,** Experimental outline for intrathoracic injection of
811 *Myh6*^{WT}~~h403/+~~ or *Myh6*$^{h403/+}$ mice with saline or dual AAV9 ABE at P0 followed by serial

812 echocardiograms. Chow diet supplemented with 0.1% Cyclosporine A was given at 5 weeks of
813 age for 11 weeks. **c-h,** Left ventricular anterior wall thickness at diastole (**c**), left ventricular
814 posterior wall thickness at diastole (**d**), left ventricular internal diameter at diastole (**e**) and systole
815 (**f**), ejection fraction (**g**), and fractional shortening (**h**), of *Myh6*^{WT} mice, *Myh6*$^{h403/+}$ mice, or ABE-
816 treated *Myh6*$^{h403/+}$ mice at 16 weeks of age. *n*=5 for each group. Data are mean ± s.e.m. **i,**
817 Representative Masson's trichrome staining of serial (500 μm interval) transverse sections for
818 *Myh6*^{WT} mice, *Myh6*$^{h403/+}$ mice, or ABE-treated *Myh6*$^{h403/+}$ mice at 16 weeks of age. Scale bar, 1
819 mm. **j,** Ventricular cross-sectional area measurements from *n*=3-5 mice for each experimental
820 group. Data are mean ± s.d. **k,** Average wall thickness measurements from *n*=3-5 mice for each
821 experimental group. Data are mean ± s.d. **l,** Heart weight (HW) to tibia length (TL) measurements
822 from *n*=5 mice for each experimental group. Data are mean ± s.d. **m,** Percentage of collagen area
823 *n*=3-5 mice for each experimental group. Data are mean ± s.d. **P* < 0.05, ***P* < 0.01 by Student's
824 unpaired two-sided *t*-test.

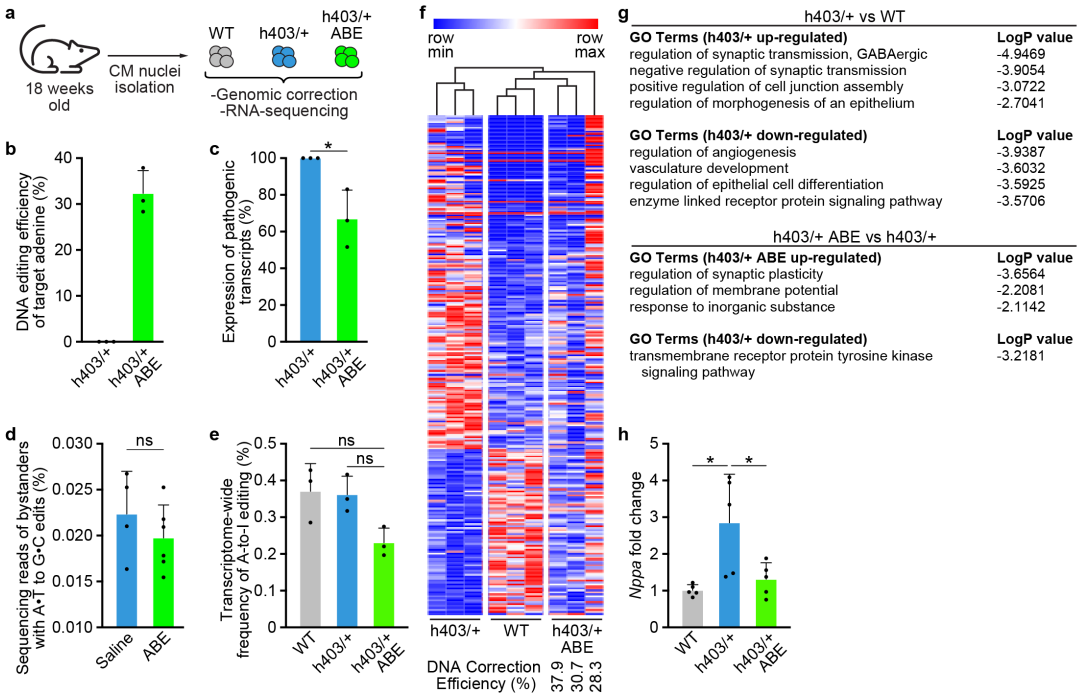

Fig. 5: Genomic and transcriptomic changes following dual AAV9 ABE injection in mice. **a,** Cardiomyocyte nuclei were isolated from ventricles of 18 weeks old *Myh6*^{WT} mice, *Myh6*$^{h403/+}$ mice, or ABE-treated *Myh6*$^{h403/+}$ mice to assess genomic correction and transcriptomic changes. **b,** DNA-editing efficiency for correcting the pathogenic adenine nucleotide following dual AAV9 ABE treatment. Data are mean ± s.d. **c,** Percentage of expressed pathogenic transcripts in ABE-treated *Myh6*$^{h403/+}$ mice compared to Myh6$^{h403/+}$ mice. Data are mean ± s.d. **d,** Bystander editing in ABE-treated *Myh6*$^{h403/+}$ mice compared to saline-treated mice. Data are mean ± s.d. **e,** Transcriptome-wide nuclear levels of A-to-I RNA editing in *Myh6*^{WT} mice, *Myh6*$^{h403/+}$ mice, and ABE-treated *Myh6*$^{h403/+}$ mice. Data are mean ± s.d. **f,** Heat map of 257 differentially expressed genes amongst *Myh6*^{WT} or *Myh6*$^{h403/+}$ mice and ABE-treated *Myh6*$^{h403/+}$ mice. Samples and genes are ordered by hierarchical clustering. Data was scaled by the sum of each row and are displayed as row min and row max. ABE-treated *Myh6*$^{h403/+}$ mice cluster with *Myh6*^{WT} mice. Editing efficiency for each ABE-treated *Myh6*$^{h403/+}$ mouse is indicated. **g,** Top gene ontology (GO) terms

839 associated with the differentially expressed genes in the comparison of h403/+ vs WT (top) and
840 h403/+ ABE-treated vs h403/+ (bottom). **h,** Fold change expression of *Nppa* mRNA expression
841 for $Myh6^{h403/+}$ mice and ABE-treated $Myh6^{h403/+}$ mice normalized to $Myh6^{WT}$ mice. Data from
842 RNA-seq and qPCR. Data are mean ± s.d. For all: $*P < 0.05$ by Student's unpaired two-sided *t*-
843 test, n=3 biological replicates for each group.

Echocardiography Measurements

	LVAW;d (mm)			P Value		
	WT	h403/+	ABE h403/+	h403/+ vs WT	ABE h403/+ vs WT	ABE h403/+ vs h403/+
8w	0.796 ± 0.0453	0.908 ± 0.0283	0.775 ± 0.0510	0.069	0.757	0.051
12w	0.908 ± 0.0434	1.07 ± 0.0428	0.829 ± 0.0243	**0.023**	0.154	**0.001**
16w	0.883 ± 0.0441	1.07 ± 0.0443	0.950 ± 0.0414	**0.017**	0.299	0.084

	LVID;d (mm)			P Value		
	WT	h403/+	ABE h403/+	h403/+ vs WT	ABE h403/+ vs WT	ABE h403/+ vs h403/+
8w	2.83 ± 0.126	2.54 ± 0.110	2.64 ± 0.0749	0.069	0.757	0.051
12w	2.90 ± 0.0983	2.45 ± 0.0986	2.84 ± 0.149	**0.013**	0.763	0.060
16w	2.81 ± 0.0540	2.34 ± 0.142	2.78 ± 0.110	**0.015**	0.844	**0.038**

	LVID;s (mm)			P Value		
	WT	h403/+	ABE h403/+	h403/+ vs WT	ABE h403/+ vs WT	ABE h403/+ vs h403/+
8w	1.27 ± 0.109	1.05 ± 0.0580	1.20 ± 0.0988	0.107	0.638	0.222
12w	1.37 ± 0.0729	1.00 ± 0.0544	1.16 ± 0.0794	**0.004**	0.085	0.147
16w	1.24 ± 0.0520	0.940 ± 0.0713	1.21 ± 0.108	**0.010**	0.829	0.071

	LVPW;d (mm)			P Value		
	WT	h403/+	ABE h403/+	h403/+ vs WT	ABE h403/+ vs WT	ABE h403/+ vs h403/+
8w	0.850 ± 0.0349	0.899 ± 0.0262	0.771 ± 0.0695	0.300	0.335	0.123
12w	0.910 ± 0.0471	1.00 ± 0.0605	0.807 ± 0.0546	0.264	0.192	**0.044**
16w	0.867 ± 0.0590	1.04 ± 0.0809	0.970 ± 0.0709	0.128	0.299	0.548

	EF (%)			P Value		
	WT	h403/+	ABE h403/+	h403/+ vs WT	ABE h403/+ vs WT	ABE h403/+ vs h403/+
8w	87.0 ± 1.79	88.6 ± 0.606	86.8 ± 1.86	0.428	0.922	0.374
12w	85.8 ± 2.01	89.4 ± 1.40	88.2 ± 2.13	0.188	0.448	0.652
16w	87.4 ± 1.63	91.7 ± 0.807	87.3 ± 1.61	**0.045**	0.965	**0.039**

	FS (%)			P Value		
	WT	h403/+	ABE h403/+	h403/+ vs WT	ABE h403/+ vs WT	ABE h403/+ vs h403/+
8w	55.4 ± 2.19	56.7 ± 0.894	52.6 ± 3.30	0.592	0.509	0.269
12w	53.9 ± 2.40	58.1 ± 2.25	57.1 ± 2.79	0.238	0.404	0.798
16w	55.8 ± 2.33	61.6 ± 1.40	55.5 ± 2.12	0.066	0.928	**0.043**

Table 1: Summary of echocardiographic measurements for humanized mice. Echocardiographic measurements in *Myh6*^{WT} mice, *Myh6*$^{h403/+}$ mice, and ABE-treated *Myh6*$^{h403/+}$ mice (8-16 weeks, n=5) for changes in left ventricular anterior wall thickness (LVAW), left ventricular internal diameter at diastole (LVID;d) and at systole (LVID;s), left ventricular posterior wall thickness (LVPW), ejection fraction (EF) and fractional shortening (FS). *P* values are calculated by Student's unpaired two-sided *t*-test for given comparisons. *P* values <0.05 are in bold. Data are mean ± s.e.m.

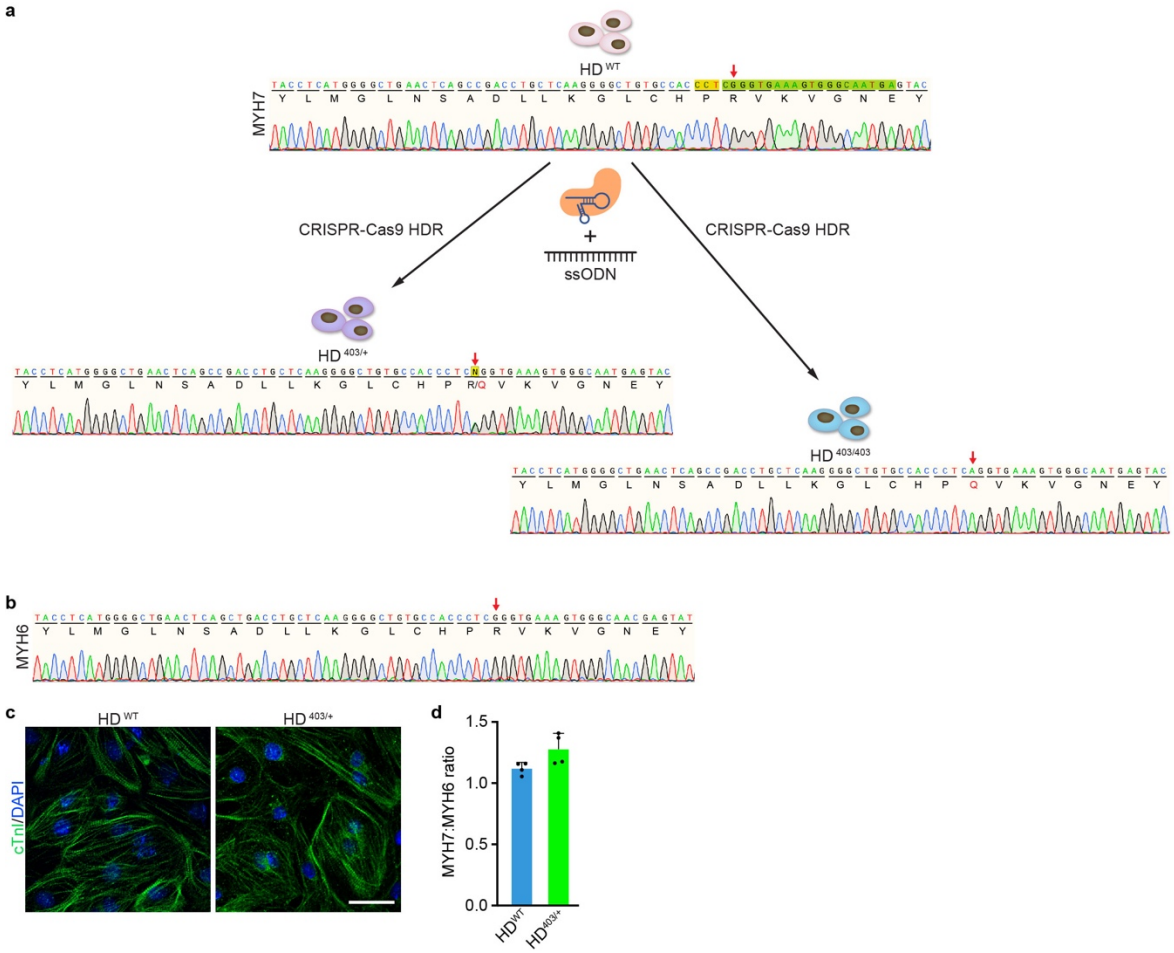

853

854 **Extended Data Fig. 1: Generation of isogenic HD$^{403/+}$ and HD$^{403/403}$ iPSCs by homology-**
855 **directed repair. a,** Using iPSCs derived from a healthy donor (HD^{WT}), the *MYH7* p.R403Q
856 (c.1208G>A) variant was introduced by CRISPR-Cas9-based homology-directed repair (HDR)
857 using SpCas9, a sgRNA (spacer sequence colored in green, PAM sequence colored in gold), and
858 a single-stranded oligodeoxynucleotide (ssODN) donor template containing the pathogenic
859 variant. A heterozygous genotype (HD$^{403/+}$) and homozygous genotype (HD$^{403/403}$) were isolated.
860 Chromatograms highlighting insertion of the pathogenic variant and corresponding amino acid
861 changes are shown for indicated genotypes. Red arrows indicate coding nucleotide 1208 and amino
862 acid 403. **b,** Sanger sequencing chromatogram showing no insertion of the pathogenic variant on
863 the highly homologous *MYH6* gene. Red arrow indicates coding nucleotide 1211 and amino acid

864 404. **c,** HD^{WT} and $HD^{403/+}$ iPSCs readily differentiate into CMs. Cardiac troponin I (cTnI, green)
865 highlights CMs; nuclei (blue) are marked by DAPI (4',6-diamidino-2-phenylindole). Scale bar, 25
866 μm. **d,** Ratio of *MYH7* to *MYH6* gene expression in HD^{WT} and $HD^{403/+}$ iPSC-CMs as measured by
867 quantitative PCR. Data are mean ± s.d.

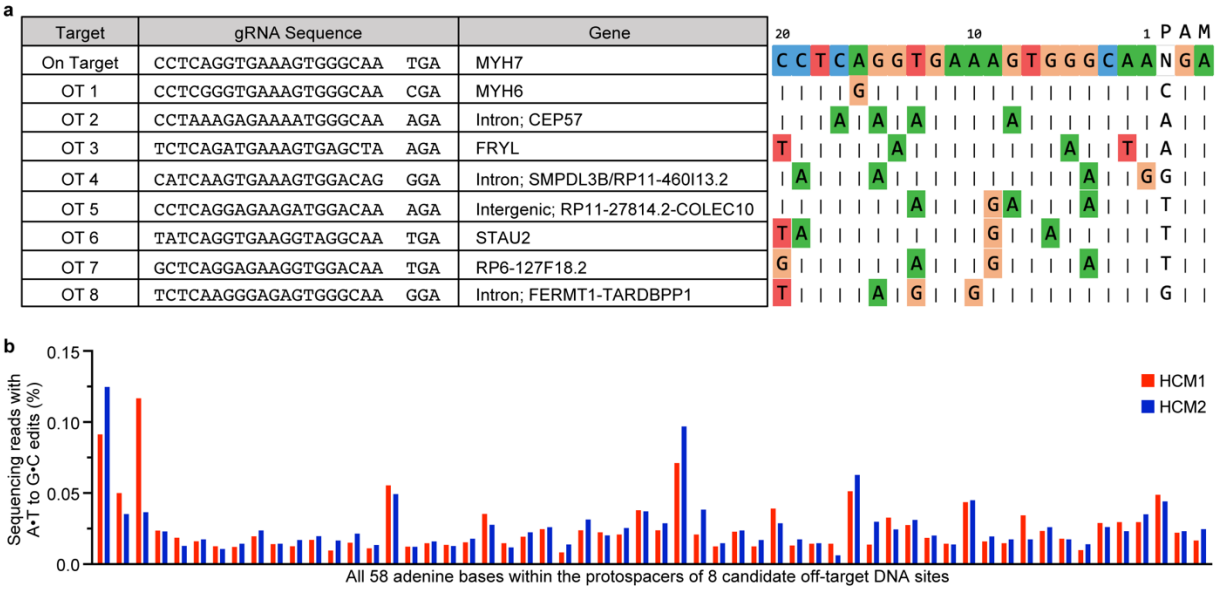

Extended Data Fig. 2: Computationally determined off-target sites for h403_sgRNA with ABEmax-VRQR. a, Genomic loci of eight candidate off-target sequences (left) and alignments of eight candidate off-target sites to the on-target protospacer (right). Nucleotides that match the protospacer are indicated with a vertical dash. Nucleotides that differ are shown for each site. Numbering of nucleotides in protospacer starts with the nucleotide immediately 5' of the PAM as nucleotide 1. **b,** ~~Deep~~ High throughput sequencing (HTS) to measure editing for all 58 adenines within the protospacers of the top eight CRISPOR-identified candidate off-target loci. ~~Deep sequencing~~ HTS was performed for ABE-treated *MYH7*$^{403/+}$ HCM1, and *MYH7*$^{403/+}$ HCM2 iPSCs.

```
Mouse      DADKSAYLMGLNSADLLKGLCHPQVKVGNEYVTKGQS  37
Human      EADKSAYLMGLNSADLLKGLCHPQVKVGNEYVTKGQN  37
           :**********************************.
                                 ↑
                                403

           D  A  D  K  S  A  Y  L  M  G  L  N  S  A  D  L  L  K  G  L
Mouse      GATGCTGACAAATCAGCCTACCTTATGGGGCTGAACTCAGCTGACCTGCTCAAGGGCCTG  60
Human      GAGGCTGACAAGTCTGCCTACCTCATGGGGCTGAACTCAGCCGACCTGCTCAAGGGGCTG  60
           E  A  D  K  S  A  Y  L  M  G  L  N  S  A  D  L  L  K  G  L
           ** ******** ** ******** ***************** ************** ***

           C  H  P  Q  V  K  V  G  N  E  Y  V  T  K  G  Q  S
Mouse      TGTCACCCTCAGGTGAAGGTGGGGAACGAGTATGTCACCAAGGGGCAGAGT  111
Human      TGCCACCCTCAGGTGAAAGTGGGCAATGAGTACGTCACCAAGGGGCAGAAT  111
           C  H  P  Q  V  K  V  G  N  E  Y  V  T  K  G  Q  N
           ** ***************** ***** ** ****** **************** *
                  ↑
           c.1208G>A
```

Extended Data Fig. 3: Comparison of mouse and human myosin heavy chain sequences. Homology comparison for mouse α-myosin heavy chain (*Myh6*) and human β-myosin heavy chain (*MYH7*) at the amino acid level (top) and DNA sequence level (bottom) around glutamine 403. The h403_sgRNA is illustrated in green and the PAM sequence is illustrated in yellow. The pathogenic c.1208 G>A variant is located at position 16 within the canonical base editing window of positions 14-17, counting the adenine nucleotide immediately 5' of the PAM as position 1.

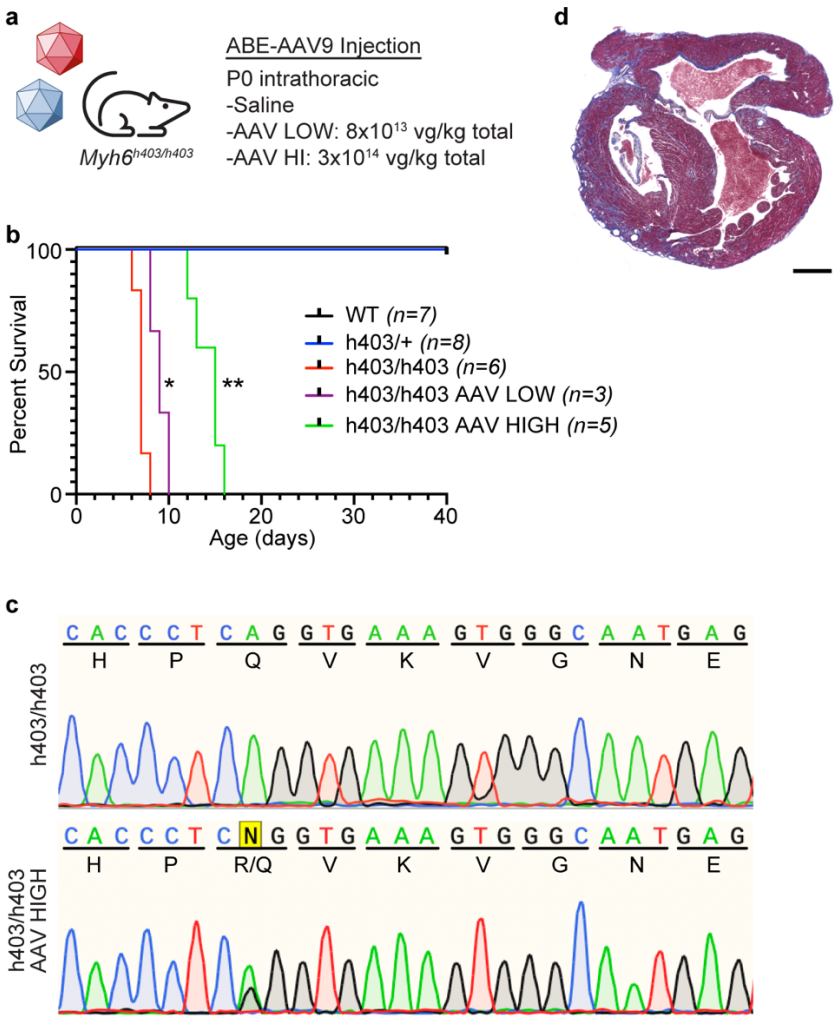

Extended Data Fig. 4: Validation of a dual AAV9 ABE system in mice. a, Injection details for treating *Myh6*$^{h403/h403}$ mice with ABE-AAV9 or saline. **b,** Kaplan-Meier curve for *Myh6*^{WT} mice (n=7), *Myh6*$^{h403/+}$ mice (n=8), *Myh6*$^{h403/h403}$ mice (n=6), and ABE-treated *Myh6*$^{h403/h403}$ mice at a low (AAV LOW, n=3) or high dose (AAV HIGH, n=5). Median lifespans: *Myh6*^{WT} and *Myh6*$^{h403/+}$ mice, >40 days; *Myh6*$^{h403/h403}$ mice, 7 days; AAV LOW *Myh6*$^{h403/h403}$ mice, 9 days (1.3-fold longer, $P < 0.05$); AAV HIGH *Myh6*$^{h403/h403}$ mice, 15 days (2.1-fold longer, $P < 0.01$). **c,** Sanger sequencing chromatograms for a *Myh6*$^{h403/h403}$ mouse and a AAV HIGH *Myh6*$^{h403/h403}$ mouse showing 35% on-target editing of the target pathogenic adenine at the cDNA level. **d,** Four-

chamber sectioning and Masson's trichrome staining of a AAV HIGH *Myh6*$^{h403/h403}$ mouse at 15 days ~~old~~of age. *$P < 0.05$, **$P < 0.01$ by Mantel-Cox test.

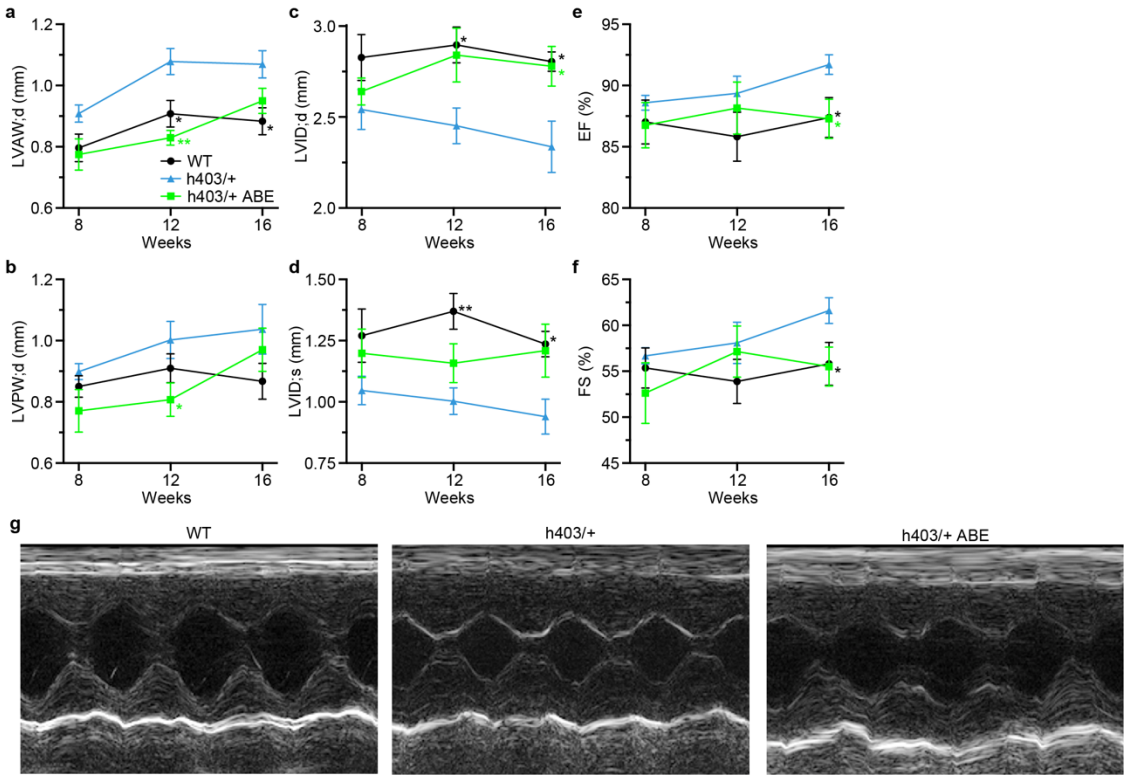

Extended Data Fig. 5: Serial echocardiograms following dual AAV9 ABE editing of *Myh6*$^{h403/+}$ mice. a-f, Left ventricular anterior wall thickness at diastole (**a**) left ventricular posterior wall thickness at diastole (**b**), left ventricular internal diameter at diastole (**c**) and systole (**d**), ejection fraction (**e**), and fractional shortening (**f**), of *Myh6*^{WT} mice, *Myh6*$^{h403/+}$ mice, or ABE-treated *Myh6*$^{h403/+}$ mice from 8-16 weeks of age. *n*=5 for each group. Data are mean ± s.e.m. *$P < 0.05$, **$P < 0.01$ by Student's unpaired two-sided *t*-test for *Myh6*^{WT} mice compared to *Myh6*$^{h403/+}$ mice (black) and ABE-treated *Myh6*$^{h403/+}$ mice compared to *Myh6*$^{h403/+}$ mice (green). **g,** Representative M-mode images for *Myh6*^{WT} mice, *Myh6*$^{h403/+}$ mice, and ABE-treated *Myh6*$^{h403/+}$ mice at 16 weeks of age.

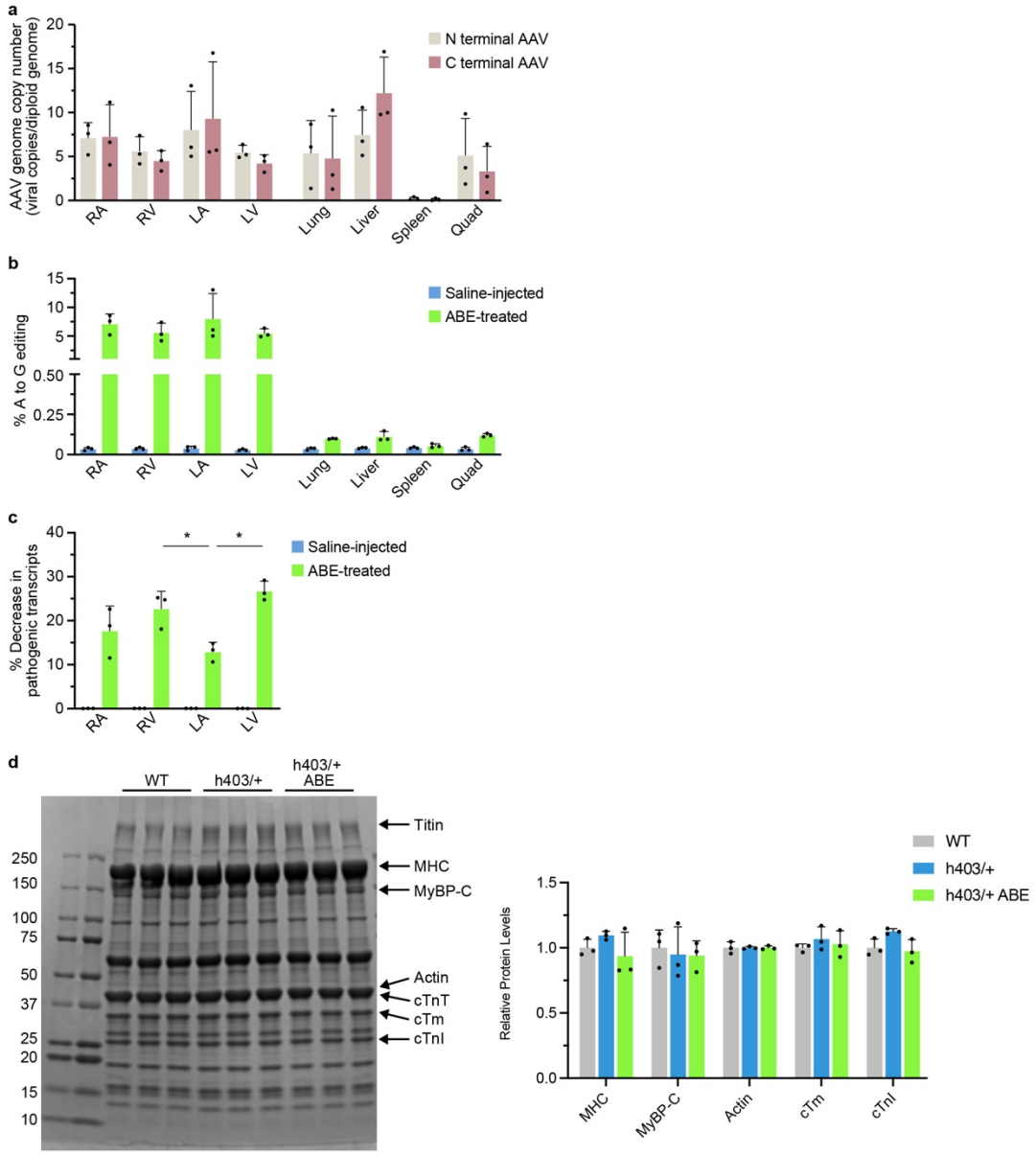

908

909 **Extended Data Fig. 6: Genomic and proteomic analysis of select tissues following dual AAV**
910 **ABE editing. a,** Viral copy numbers for the N terminal AAV and C terminal AAV were quantified
911 from the right atrium (RA), right ventricle (RV), left atrium (LA), left ventricle (LV), lung, liver,
912 spleen, and quadriceps muscle (Quad) from ABE-treated *Myh6*$^{h403/+}$ mice at 16 weeks of age. **b,**
913 The percentage of A to G editing was determined by high throughput sequencing (HTS) of
914 genomic DNA in the RA, RV, LA, LV, lung, liver, spleen, and Quad from ABE-treated and saline-

915 injected *Myh6*$^{h403/+}$ mice. **c,** The percentage decrease in mutant transcripts in the RA, RV, LA, and
916 LV was determined by HTS of cDNA from ABE-treated and saline-injected *Myh6*$^{h403/+}$ mice. **d,**
917 Cardiac myofibrils were isolated from *Myh6*^{WT} mice, *Myh6*$^{h403/+}$ mice, and ABE-treated *Myh6*$^{h403/+}$
918 mice, run on a 4-20% polyacrylamide gel, and stained with Coomassie G-250. Key sarcomeric
919 proteins are marked, including titin, myosin heavy chain (MHC), myosin binding protein C
920 (MyBP-C), actin, cardiac troponin T (cTnT), cardiac tropomyosin (cTm), and cardiac troponin I
921 (cTnI). Sizes for ladder markings are in kDa. Relative protein amounts for each key sarcomeric
922 protein are normalized to WT. Data are mean ± s.d. *$P < 0.05$ by Student's unpaired two-sided *t*-
923 test, *n*=3 biological replicates for each group.
924

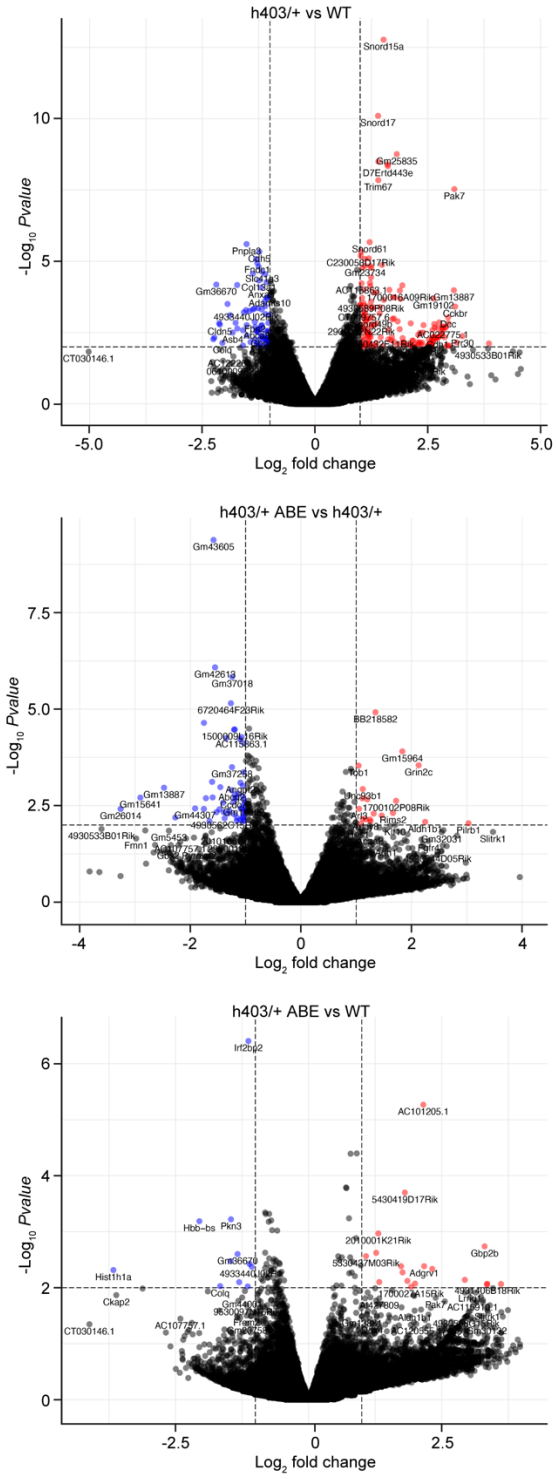

925

926 **Extended Data Fig. 7: RNA-sequencing analysis of dual AAV9 ABE editing of *Myh6*$^{h403/+}$**

927 **mice.** Volcano plot showing fold-change and *p*-value of genes up-regulated (red) and down-

928 regulated (blue) in *Myh6*$^{h403/+}$ mice compared to *Myh6*^{WT} mice (top), ABE-treated *Myh6*$^{h403/+}$ mice
929 compared to *Myh6*$^{h403/+}$ mice (middle), and ABE-treated *Myh6*$^{h403/+}$ mice compared to *Myh6*^{WT}
930 mice (bottom).
931

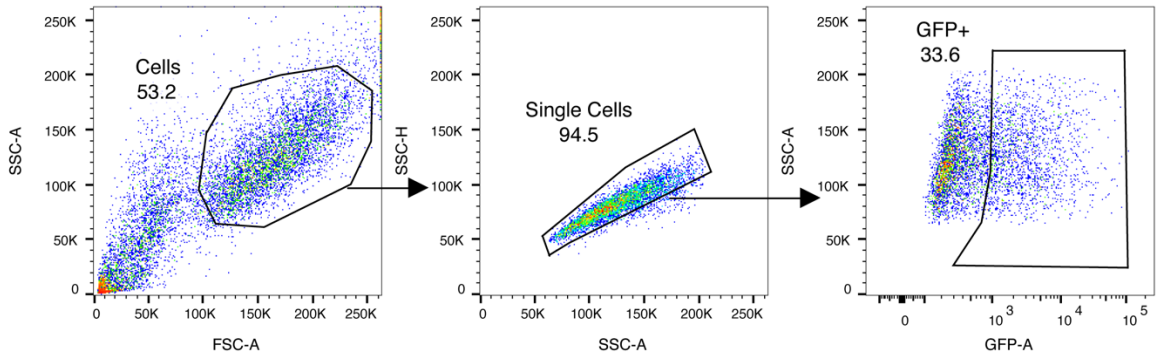

Supplementary Figure 1. Representative flow cytometry gating strategy for GFP+ iPSCs. For generation of isogenic iPSCs containing the *MYH7* c.1208 G>A (p.R403Q) mutation via homology-directed repair, and for base editing correction of the *MYH7* c.1208 G>A (p.R403Q) mutation, iPSCs were nucleofected with a single plasmid encoding ~~for~~ Cas9 nuclease or an adenine base editor linked to GFP via a 2A self-cleaving peptide, and the sgRNA of interest. Cells that were successfully nucleofected with the gene editing components express GFP, and single GFP+ iPSCs were collected.

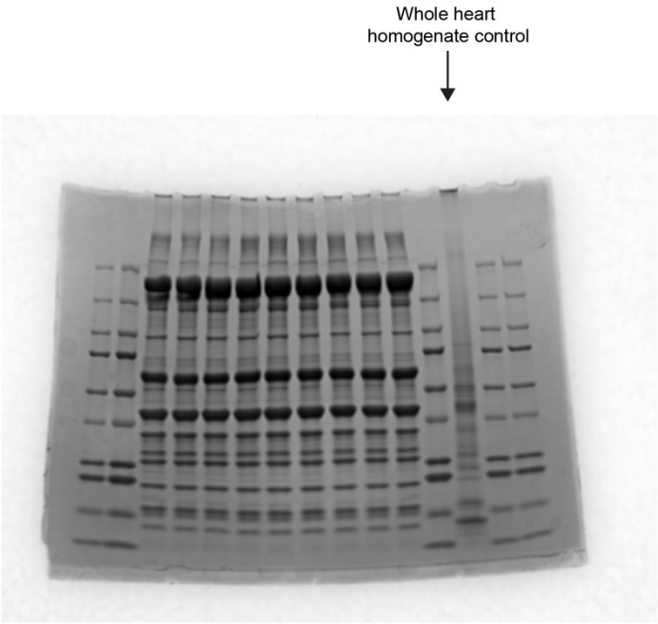

941

942 **Supplementary Figure 2. Uncut gels.** Full unedited gel for Extended Data Fig 6.

943

944 **Supplementary Table 1. Summary of oligos**

Oligo Name	Oligo Sequence
sgRNA for HDR Knock-In of MYH7 R403Q	TCATTGCCCACTTTCACCCG
ssODN for HDR Knock-In of MYH7 R403Q	TGCTACTTGCCTTTTCCTTCCAGAGGCTGACAAGTCTGCCTACCTCATGGGGCTGAACTCAGCCGACCTGCTCAAGGGGCTGTGCCACCCTCAGGTGAAAGTGGGCAATGAGTACGTCACCAAGGGGCAG
Sequencing for hMYH7 F	ACCTCCACATCCTGGGTTCAA
Sequencing for hMYH7 R	GTGGAGGAGAGACCCATATT
Sequencing for hMYH6 F	GGAGGCTGTAGTGAGCCAAG
Sequencing for hMYH6 R	AGGAGCAAGCGAGTGATTGT
h403_sgRNA	CCGCAGGTGAAAGTGGGCAA
HTS ON-Target F	TCGTCGGCAGCGTCAGATGTGTATAAGAGACAGTCCTCTCATACACTGCCTTGG
HTS ON-Target R	GTCTCGTGGGCTCGGAGATGTGTATAAGAGACAGCACCATGCCTGGCTAATTTT
HTS OFF1 F	TCGTCGGCAGCGTCAGATGTGTATAAGAGACAGGGGACAATGACTGCCTCTGT
HTS OFF1 R	GTCTCGTGGGCTCGGAGATGTGTATAAGAGACAGTACCTCATGGGGCTGAACTC
HTS OFF2 F	TCGTCGGCAGCGTCAGATGTGTATAAGAGACAGCAGGTCTCGATTCCAAGGAG
HTS OFF2 R	GTCTCGTGGGCTCGGAGATGTGTATAAGAGACAGGCACAACCCACAAGTTTGTTT
HTS OFF3 F	TCGTCGGCAGCGTCAGATGTGTATAAGAGACAGTTTTCAAAATATTCCTGCTCACT
HTS OFF3 R	GTCTCGTGGGCTCGGAGATGTGTATAAGAGACAGAGGCACCTTTCTGTGTGCTT
HTS OFF4 F	TCGTCGGCAGCGTCAGATGTGTATAAGAGACAGATTCTGGATGCAGGATTTGC
HTS OFF4 R	GTCTCGTGGGCTCGGAGATGTGTATAAGAGACAGGTGGACAACAGGCCACTCTT
HTS OFF5 F	TCGTCGGCAGCGTCAGATGTGTATAAGAGACAGGGACAATTTGTATTTTAGCTTATTTTC
HTS OFF5 R	GTCTCGTGGGCTCGGAGATGTGTATAAGAGACAGTCCCCTGCTTTTCTCTGTGT
HTS OFF6 F	TCGTCGGCAGCGTCAGATGTGTATAAGAGACAGTGATCCTGAAGATTAGTGGATGC
HTS OFF6 R	GTCTCGTGGGCTCGGAGATGTGTATAAGAGACAGCCATCCTGAGATAATCCTCCA
HTS OFF7 F	TCGTCGGCAGCGTCAGATGTGTATAAGAGACAGACCTAGGAGGCTGGGATTGT
HTS OFF7 R	GTCTCGTGGGCTCGGAGATGTGTATAAGAGACAGCATGACAAGGAGTCCGAGGT
HTS OFF8 F	TCGTCGGCAGCGTCAGATGTGTATAAGAGACAGGCCCCTGGTTACAGCATAAG
HTS OFF8 R	GTCTCGTGGGCTCGGAGATGTGTATAAGAGACAGCCACAACCACTGACTGACTGA
sgRNA for Knock-In of MYH7 R403Q into murine Myh6	TCGTTCCCCACCTTCACCCG

ssODN for Knock-In of MYH7 R403Q into murine Myh6	TGGGACAAAGGAATGGAGGTACTGAAAATGCTTCCCCTCTCCTTGTCTATCAGAT GCTGACAAATCAGCCTACCTCATGGGGCTGAACTCAGCCGACCTGCTCAAGGGG CTGTGCCACCCTCAGGTGAAAGTGGGCAATGAGTACGTCACCAAGGGGCAGAGT GTACAGCAAGTGTACTAT
Genotyping for Myh6 F	GAGAAGCAGTGGTCATCATC
Genotyping for Myh6 R	GTGAGAAACACGTGGTGTCC
HTS Myh6 On-Target F	TCGTCGGCAGCGTCAGATGTGTATAAGAGACAGGGATCAAGGACATGGCAAAT
HTS Myh6 On-Target R	GTCTCGTGGGCTCGGAGATGTGTATAAGAGACAGGCTTGGTCTCCAGGGTTG
HTS Myh6 cDNA On-Target F	TCGTCGGCAGCGTCAGATGTGTATAAGAGACAGGATGGCACAGAAGATGCTGA
HTS Myh6 cDNA On-Target R	GTCTCGTGGGCTCGGAGATGTGTATAAGAGACAGCGAACATGTGGTGGTTGAAG
Sanger Myh6 cDNA On-Target F	GCTCTTGGCCACTGATAGTGC
Sanger Myh6 cDNA On-Target R	GCTCAAAGCTGTTGAAATCG
VCN N terminal AAV half F	ACCAGAAAGAGCGAGGAAAC
VCN N terminal AAV half R	TCGTTGGGCAGGTTCTTATC
VCN N terminal AAV Probe	/56-FAM/TTGGTCATC/ZEN/CGCTCGATGAAGCTC/3IABkFQ/
VCN C terminal AAV half F	CCCAAGAGGAACAGCGATAAG
VCN C terminal AAV half R	CCACCACCAGCACAGAATAG
VCN C terminal AAV Probe	/56-FAM/ATCGCCAGA/ZEN/AAGAAGGACTGGGAC/3IABkFQ/

945